

國立交通大學

顯示科技研究所

碩士論文

反射式電子紙之色彩特性化研究：
以膽固醇液晶顯示器為例



Colorimetric Characterization of Reflective E-paper:

A Case Study of ChLCD

研究生：鍾岳

指導教授：田仲豪 博士

中華民國一百年八月

反射式電子紙之色彩特性化研究：

以膽固醇液晶顯示器為例

Colorimetric Characterization of Reflective E-paper:

A Case Study of ChLCD

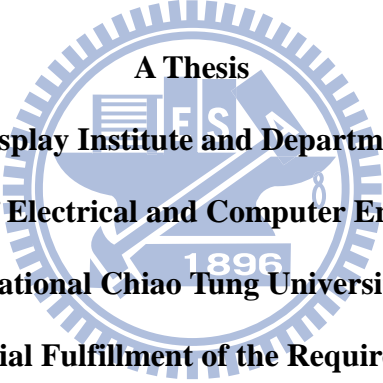
研究生：鍾岳

Student: Yueh Chung

指導教授：田仲豪

Advisor: Chung-Hao Tien

國立交通大學
顯示科技研究所
碩士論文



A Thesis
Submitted to Display Institute and Department of Photonics
College of Electrical and Computer Engineering
National Chiao Tung University
in partial Fulfillment of the Requirements
for the Degree of
Master
in
Display Institute
August 2011

Hsinchu, Taiwan, Republic of China

中華民國一百年八月

反射式電子紙之色彩特性化研究： 以膽固醇液晶顯示器為例

碩士研究生：鍾岳 指導教授：田仲豪

國立交通大學
顯示科技研究所

摘要

對於彩色圖像傳播而言，為確保影像與色彩的真實性，顯色媒介的色彩特性化是必要的工作之一。在本篇論文中將會介紹各種色彩特性化方法：物理模式、應用數值迴歸模式、利用內插法的對照表模式等。由於電子紙這種新型顯色媒介的興起，本論文以反射式膽固醇液晶顯示器為例，完成以上三種方法的色彩特性化的建立。此外，不同方法的可行性與精確度會被討論與檢驗。依照實驗結果與理論的比較，膽固醇液晶具有複雜的顯色物理機制，物理模式不適用於色彩特性化。又因膽固醇液晶顯示器的色彩空間與非設備從屬色彩空間(CIE XYZ)存在著高度非線性，較低階數值迴歸模式(20 個多項式參數、729 training data)，其精準度約 $\Delta E_{00_avg.} \sim 1.4$ ，仍大於一般的標準($\Delta E_{00} < 1$)。對照表模式中不均勻的區間取樣(packing)是和膽固醇液晶顯示器本身顯色非線性的特性吻合，利用 729 點四面體內差法的對照表模式色彩特性化，將能夠達到高度的精確性($\Delta E_{00_avg.} = 0.79$)。

Colorimetric Characterization of Reflective E-paper: A Case Study of ChLCD

Master student: Yueh Chung

Advisor: Dr. Chung-Hao Tien

**Display Institute
National Chiao Tung University**

Abstract

Colorimetric characterization of information devices is essential among the image communication. The upcoming electronic papers developed by the various ingenuities also need reliable color models. Therefore, general procedures: physical model, numerical model with regression, and look-up table with interpolation for characterizing any potential e-Paper technologies were introduced in this study. One of the commercial e-Paper products, cholesteric liquid crystal display (ChLCD) would be used as a test example to verify corresponding colorimetric characterization based on the three proposed methodologies. In addition, the feasibility and the fidelity of different manners would also be examined and discussed. In accordance with the experiment, physical model is impractical for ChLCD due to its inherent complex operating mechanism. Because of the nonlinearity between ChLCD color space and CIEXYZ space, the accuracy from a feasible numerical model with regression (20 polynomial terms and 729 training data) is reached to $\Delta E_{00_avg.}=1.4$, which is still larger than indistinguishable criterion ($\Delta E_{00}<1$). Compared with physical and numerical modeling, if the non-uniform packing is in response to the features of ChLCD itself, the colorimetric characterization utilizing 729 look-up tables with tetrahedral interpolation can offer the prediction with high fidelity ($\Delta E_{00_avg.}=0.79$).

誌謝

首先，我想先感謝我的指導教授田仲豪這幾年來在大學專題上以及碩士班研究上無私的諄諄教誨與指導，使得我在色彩這塊領域有一定程度的了解，也能順利完成碩士班的學業與此篇論文。

在實驗室中，我最先要感謝的是這兩年多來一直帶領我成長直到畢業的陸彥行學長，沒有您的幫助，我可能沒有辦法如此順利畢業。還要特別感謝藍子翔學長在我專題時如此有耐心地教導我。在此祝福以上兩位學長近期都能順利畢業。還有要感謝剛生完小孩的鄭璧如學姊，謝謝您在課業之餘教導我許多人生觀念。另外，還要感謝簡銘進，洪健翔，蔡玉麟學長，謝謝你們對於我學業以及生活上的幫助。另外，也感謝一路陪伴我到畢業的議寬還有學弟妹國恩、杰恩、孟潔。希望這三位學弟學妹明年也能順利畢業。還有其他已經畢業的學長姐們，謝謝你們。再額外感謝我的大學以及研究所同學林至宏，謝謝你那時帶我進田老師實驗室，這裡真的是臥虎藏龍啊！

最後，當然得感謝我最親愛的家人，謝謝你們在家裡默默地支持我、鼓勵我，能讓我無後顧之憂地完成碩士班的學業。還要感謝我的朋友們，因為一路有你們的陪伴，讓我的學習之路並不孤單。在此，我將畢業的這份喜悅分享給曾經幫助過我的諸位。

Table of Contents

Abstract(Chinese)	i
Abstract(English)	ii
Acknowledgement	iii
Table of Contents	iv
Figure Captions	vi
Table Captions	ix
Chapter 1 Introduction	1
1.1 Preface.....	1
1.2 Preview of color modeling	5
1.3 Motivation and Organization	8
Chapter 2 Colorimetric Characterization Methods	10
2.1 The framework of colorimetric characterization	10
2.2 Physical model	12
2.3 Numerical model.....	16
2.4 Look-up table with interpolation	20
2.4.1 Examples of 3-D interpolation	22
2.4.2 Trilinear interpolation.....	23
2.4.3 Prism interpolation	25
2.4.4 Pyramid interpolation	26
2.4.5 Tetrahedral interpolation	27
2.4.6 Applications of 3D interpolation	31
Chapter 3 Colorimetric Characterization on ChLCD	32

3.1 Introduction of cholesteric liquid crystal	32
3.1.1 Optical characteristics in different textures	33
3.1.2 Gray scale property of cholesteric liquid crystals	34
3.2 Physical mechanism of three-layers-stacked ChLCD.....	35
3.3 Numerical method.....	37
3.4 Look-up table with interpolation	39
Chapter 4 Experiment and Verification	42
4.1 Experimental platform	42
4.2 Examination of performance in Fujitsu FLEPiA	44
4.3 Regression data with numerical model	49
4.4 Interpolation from look-up tables	53
4.5 Summary	59
Chapter 5 Conclusions and Discussions.....	61
5.1 Conclusions.....	61
5.2 Discussions	63
Reference	64



Figure Captions

Fig. 1-1 The applications of commercial e-Papers	2
Fig. 1-2 Basic structures of these four different e-Papers	5
Fig. 1-3 Three levels of color modeling: colorimetric characterization, color reproduction, human evaluation.....	6
Fig. 1-4 The elements of color reproduction	7
Fig. 1-5 An example of color transformation procedure of display system	8
Fig. 2-1 Color gamut with three primary colors	14
Fig. 2-2 Emission spectrum of trichromatic white multi-LED source with color temperature of 6500K (solid line) and gaussian fit (dashed line).....	16
Fig. 2-3 Schematic diagram of the regression method	17
Fig. 2-4 Flow chart of 3D LUT	21
Fig. 2-5 (a) Equal-partition sampling (b) Unequal-partition sampling of color space (XYZ).....	21
Fig. 2-6 Bilinear interpolation	24
Fig. 2-7 Trilinear interpolation	24
Fig. 2-8 Prism interpolation.....	25
Fig. 2-9 Pyramid interpolation.....	27
Fig. 2-10 Tetrahedral interpolation.....	28
Fig. 2-11 The tetrahedral interpolation problem.....	29
Fig. 2-12 The convex inclusion problem.....	29
Fig. 3-1 ChLC molecule structure, where P is the helical pitch with ChLC molecule rotating 360° perpendicular to Z-axis.....	32
Fig. 3-2 Schematic diagram for different textures of the ChLCs	34
Fig. 3-3 Possible field-induced texture transition channels in ChLCs	34

Fig. 3-4 The gray scale states of a ChLCs display	35
Fig. 3-5 A structure of three-layers-stacked ChLCD.....	36
Fig. 3-6 Schematic illustration of the planar texture	36
Fig. 3-7 Reflection spectrum of three-layers-stacked ChLCD (FLEPia)	37
Fig. 3-8 Flow chart to determine coefficients and polynomial terms.....	38
Fig. 3-9 The gamma curve in green channel of Fujitsu FLEPia.....	41
Fig. 3-10 Flow chart to choose numbers of packing	41
Fig. 4-1 Experimental condition figure	43
Fig. 4-2 Real construction figure of experiment.....	44
Fig. 4-3 Flow chart of experiment	44
Fig. 4-4 Normalized luminance in 256 digit count of three independent channel and gray level.....	45
Fig. 4-5 Normalized X, Y, and Z values of green channel.....	45
Fig. 4-6 Normalized reflectance of 4 digit counts in red channel	46
Fig. 4-7 Normalized reflectance of 4 digit counts in green channel.....	46
Fig. 4-8 Normalized reflectance of 4 digit counts in blue channel.....	47
Fig. 4-9 (a) x,y values in CIE color space with 32, 96, 192, and 255 digit counts of R,G,B channels and gray levels	48
Fig. 4-9 (b) x,y values in CIE color space with 32, 96, 192, and 255 digit counts of cyan, magenta, yellow.....	49
Fig. 4-10 (a) The 900 randomized test color samples	50
Fig. 4-10 (b) The 900 randomized test samples in uniform a*b* color space of Fujitsu FLEPia	50
Fig. 4-10 (c) The distributions of lightness with the 900 randomized test samples	51
Fig. 4-11 Error distributions of regression	52
Fig. 4-12 The gamma curve of G channel and the predicting gamma curves of G	

channel with 3, 5, 7, 9 selected break points and piecewise linear interpolation 55

Fig. 4-13 The distribution of CIEDE2000 color differences with trilinear interpolation 55

Fig. 4-14 The distribution of CIEDE2000 color differences with prism interpolation 56

Fig. 4-15 The distribution of CIEDE2000 color differences with pyramid interpolation 57

Fig. 4-16 The distribution of CIEDE2000 color differences with tetrahedral interpolation 57

Fig. 5-1 A diagram of ChLCD color shift..... 63

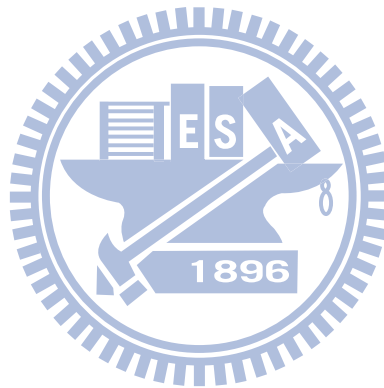


Table Captions

Table 1-1 The advantages and corresponding properties of e-Papers.....	1
Table 1-2 Performance and benchmarks in vertical electrophoretic display, electrowetting display, cholesteric liquid crystal display, and electrochromic	4
Table 2-1 The polynomials for color space conversion	18
Table 2-2 The inequality relationships and the coefficients for pyramid interpolation	26
Table 4-1 Specifications of i1 Pro	42
Table 4-2 Specifications of Fujitsu FLEPia	43
Table 4-3 Average CIEDE2000 color differences of various polynomial regressions	51
Table 4-4 The chosen packing points in cubic of 3, 5, 7, and 9 LUT	54
Table 4-5 The error between the gamma curve of Fujitsu FLEPia with green channel and the curve of packing points	54
Table 4-6 The average CIEDE2000 color differences between the measurement and predicting values of LUT	58
Table 4-7 Storage and computation cost of 3D interpolation for one component	59

Chapter 1

Introduction

1.1 Preface

In the past decade, electronic-paper (e-Paper) has become more and more noticeable due to its unique advantages, summarized in Table 1-1. The e-Paper is named from its usage overlaps in traditional paper. For example, e-Paper exhibits image content with reflection from additional illumination and keep image detail even under sunlight as well as paper. Because of the highly diffused reflectivity and excellent contrast, e-Paper is usually considered to be more comfortable to read than conventional emissive display. Furthermore, extremely low power-consumption due to the long-term image stability also has been proved in e-Paper technologies [1], and portability from thin volume, light weight, flexible and rollable form factor also has a tremendous potential to be applied in all kinds of daily consumer products [2].

Table 1-1 The advantages and corresponding properties of e-Papers

Advantages	Properties
Display	Wide viewing-angle and high contrast
Readable	Less fatigue and more comfortable
Energy savable	Low power-consumption due to reflecting operation
Portable	Thin, light, flexible, and rollable

According to the properties listed in the Table 1-1, the applications of e-Papers are expected to be applicable in time tables at bus stations, electronic pricing labels in retail shops, electronic billboards, advertisement signage, mobile phone displays, and e-readers display digital versions of books or magazines. The examples of e-Papers applications are illustrated in Fig.1-1.

e-Paper technologies can achieve these charming benefits and applications. Base on the optical switching type inside a pixel, the electro-optic devices with reflective operation can be sorted into four major categories of pixel architecture [3]:

1. Vertical colorant transposition. Colorants or reflective materials are moved or rotated from bottom to top surface for controlling the optical state, such as vertical electrophoretic display (EPD), liquid powder display, and electro-magnetic display.
2. Horizontal colorant transposition. Colorants can be moved horizontally through liquid or colored fluid to provide optical change, such as in-plane EPD, electrowetting display (EWD), electrokinetic display, and electrofluidic display.
3. Electro-optics. The transmission of optical state through a switching layer is modulated by altering optical scattering, interference or polarization, such as cholesteric liquid crystal display (ChLCD), electromechanical interference modulation display, reflective LCD, and photonic crystal display.
4. Electrochromic. The colorants undergo a chemical change that alters the light transmission, absorption, and/or reflection, such as electrochromic display.



Fig. 1-1 The applications of commercial e-Papers

The examples of operating mechanisms for the four types, vertical EPD, EWD, ChLCD, and electrochromic display, are illustrated in Fig. 1-2(a) to (d). The performances and key factors of the four techniques are compared in Table 1-2 as well. As listed in Table 1-2, vertical EPD using the E Ink technology have achieved a robust maturity of commercial products. The technique of vertical electrophoretic offers moderate reflectance with scattering appearance, bistability, and good lifetime. However, the refresh time of vertical EPD is taken too long to be suitable of video application. On the contrary, EWD has sufficient reflectance to fit the SNAP (Specifications for Newsprint Advertising Production) standard and fast switching time in dynamic operation of active matrix design. However, continuous driving leaves EWD to have a disadvantage of high power consumption. Although the optical feature of ChLCD is poorer than other types of e-Paper, ChLCD has success in outdoor usage due to the outstanding color performance under strong illumination and sunlight.

In consequence of the compared key factors in Table 1-2, while there exist

many different techniques in e-Paper, no single technology yet possesses all the features required to make e-Paper become a ubiquitous replacement for paper or for supplanting LCDs in applications. In other words, according to the specifically concerned issues of e-Readers, e-labels, multimedia, e-billboards, flexible device, and so on, different novel technologies offering sufficient capabilities will be chosen to develop the mentioned e-Paper devices. For all kinds of daily consumer products, constructing a color model is an essential work to communicate colorimetric data with high fidelity among various e-Paper technologies.

Table 1-2 Performance and benchmarks in vertical electrophoretic display, electrowetting display, cholesteric liquid crystal display, and electrochromic [3]

Types	Vertical EPD	EWD	ChLCD	Electrochromic
%R* for White or Color	40% White	55% White	30-35% Color	>50% White
Contrast Ratio	10:1	10-15:1	6:1	-
Lambertian	yes	partial	partial	yes
Voltage (V)	15	15-20	25-40	~1
Bistability	yes	no	yes	hours
Switching Speed (msec)	~100	~10	~500-700	~1
Matrix Drive	AM	AM	PM	PM
Neutral White Point	yes	yes	no	possible
Lifetime	good	unproven	good	ltd./unproven
Maturity	many products	AM demo	PM products	smart card products
Application	e-Readers, e-labels	mobile-device, billboards	billboards	smart card

*:%R: Reflectivity

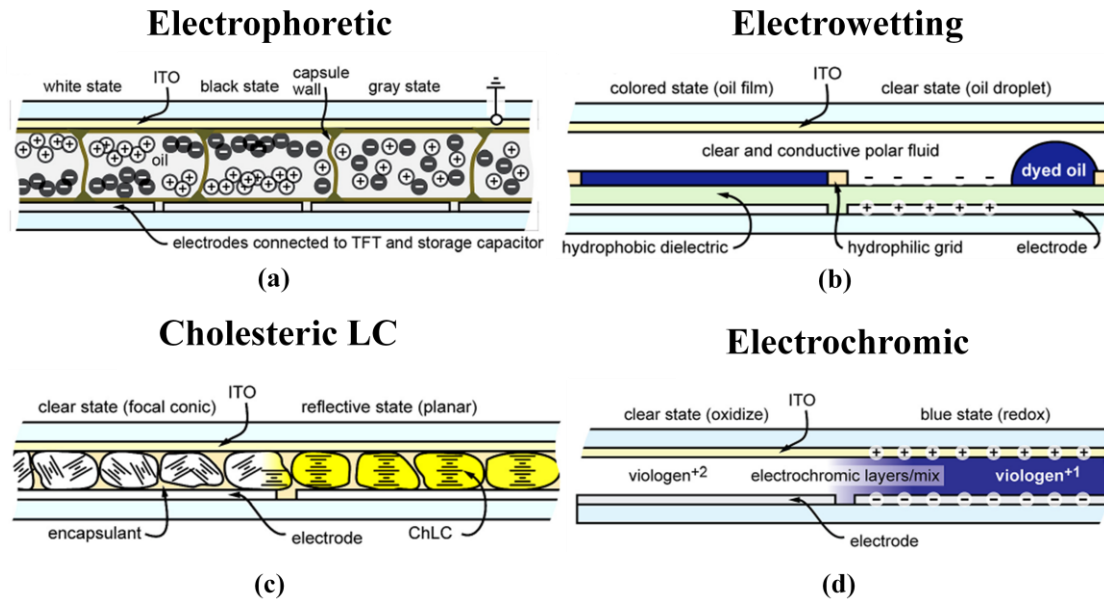


Fig. 1-2 Basic structures of these four different e-Papers [3]

1.2 Preview of color modeling

A color system can be separated into three levels including colorimetric characterization, color reproduction among various electronic multimedia, and evaluation of image quality by visual test. The flow chart of color modeling is illustrated as Fig. 1-3.

In consequence of the intrinsically colorimetric behavior subject to the operating mechanism or the adoptive material, the device-connection color space may exist an enormous discrepancy between two different devices even with identical user control signals. In order to eliminate the inconvenience of image communication, the colorimetric performance should be described with a common language in respect of standard color space. Therefore, the purpose of colorimetric characterization is to make a robust transformation between the device-connection space and the corresponding CIE colorimetry [4]. Since International Commission on Illumination (CIE) created CIE 1931 XYZ color space which is one of the first mathematically

defined color spaces in 1931, more and more studies of colorimetric characterization on different electronic devices have been developed.

Color reproduction is defined as the process by which color information from an original medium, under the original's viewing conditions, is transferred to a reproduction medium, under its viewing conditions, with the intention of the reproduction having a desired property [5], as shown in Fig. 1-4.

In terms of color reproduction, different dimensions can be identified dependent on the desired properties are concerned:

1. With reference to a reproduction only or with reference to the original and, therefore, to the relationship between the two;
2. By an application to which they relate to or to be independent of application;
3. Potentially descriptive or presenting an ideal state;
4. Measurable in quantitative terms by physical methods or expressible in qualitative terms and measurable psychovisually.

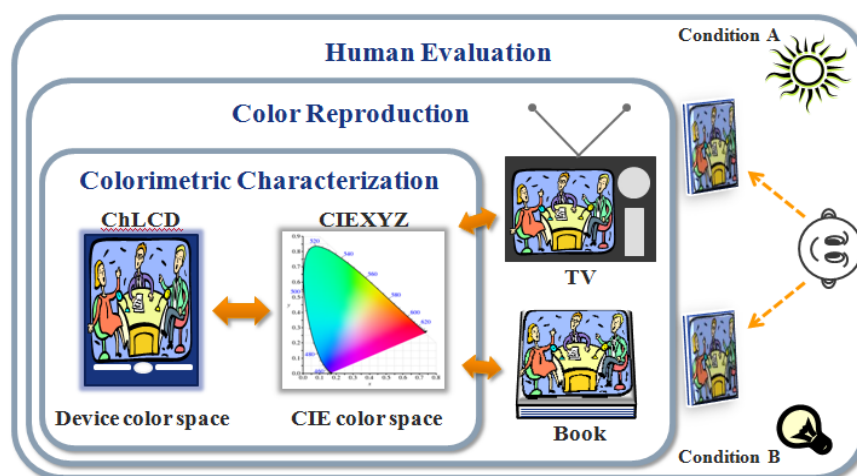


Fig. 1-3 Three levels of color modeling: colorimetric characterization, color reproduction, human evaluation

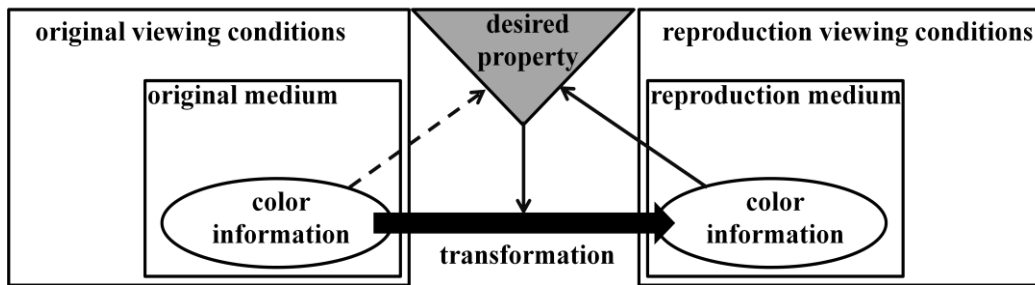


Fig. 1-4 The elements of color reproduction [5]

It is worth noting that the fourth dimension of the desired property is with respect to the evaluation of human visual test. When the different viewing conditions are introduced into the process, the reproduction of color information with high fidelity in CIE colorimetry is not equivalent to in human perception. In addition, even perceiving identical reproduction across different media, it is not represented the result of preference. Consequently, it would be beneficial to bring the psychophysical assessment into the concerned issue for achieving the best color reproduction.

In accordance with the flow chart of the color reproduction illustrated in Fig. 1-4, no matter what desired property are chosen in reproducing process, colorimetric characterization of each medium is always the fundamental step. If the colorimetric characterization is not finished yet or constructed without accuracy, another two levels of color modeling cannot progress anymore. This is the reason why colorimetric characterization is the most important work for information device.

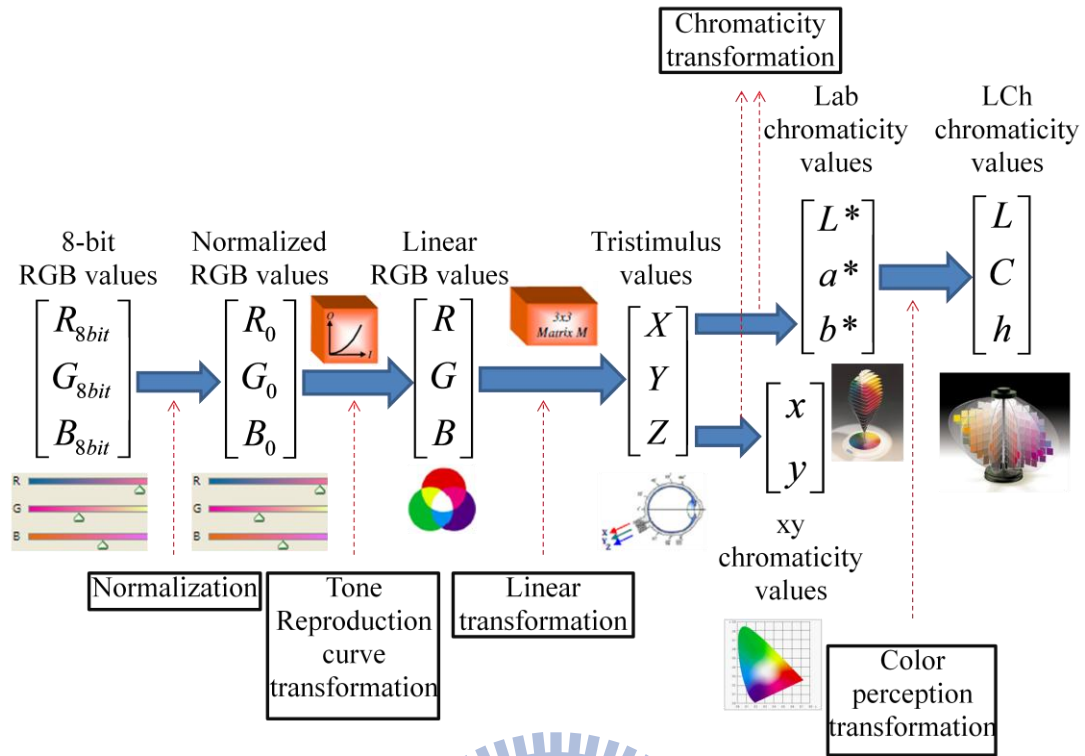


Fig. 1-5 An example of color transformation procedure of display system [6]

A color transformation procedure of a traditional display as cathode-ray-tube (CRT) or LCD is shown in Fig. 1-5. The process from RGB bit values to tristimulus or appearance value is defined as colorimetric characterization. The corresponding dataset can be reproduced to another device if and only if the characterization of the device has been completed as well. Furthermore, the physical quantities (tristimulus or chromaticity) can be further transformed into perceptual quantities (LCh) by means of the appearance model.

1.3 Motivation, Objective and Organization

In section 1.2, we have clarified the significance of colorimetric characterization for each information media. Universality of the emerging display technology, electronic paper, is also subject to robust and reliable colorimetric characterization. Unlike mature product of flat panel display such as CRT and LCD,

whose color modeling have been built up completely, e-Papers are still operated by various novel techniques but singular architecture, as introduced in section 1.1. Accordingly, in terms of various and complicated operating mechanism in e-Paper, a general rule of constructing colorimetric characterization is necessary.

In view of this, the objective of this paper is to introduce a common procedure of colorimetric characterization which can be utilized in every reflective e-Paper. We will take cholesteric liquid crystal display (ChLCD) for an examined case to illustrate how to accomplish a colorimetric characterization for a novel e-Paper following the proposed procedure. In addition, the performance of different characterizing method will be discussed for comparison as well.

In accordance with the motivation and objective, the thesis will be organized as following: in **Chapter 2**, a general procedure of colorimetric characterization including three different methods will be given. In **Chapter 3**, a full-color cholesteric liquid crystal display will be a studied case to clarify how to extend the general methods into an unknown e-Paper technology. In **Chapter 4**, the experimental results of different characterization manners applied in ChLCD will be discussed. Finally, the conclusion and discussions will be shown in **Chapter 5**.

Chapter 2

Colorimetric Characterization Methods

2.1 The framework of colorimetric characterization

Many color engineering works transports colors between imaging instruments through the medium of CIE colorimetry, and for this reason it is essential to create a model of the relationship between the device coordinates and the corresponding CIE colorimetry. There are three basic ways for generating device models:

1. Physical models (or color-mixing models) which include terms for different physical properties of the device, such as scattering, absorbance, and reflectance of colorant and substrates.
2. Numerical models in which a series of coefficients is defined, usually by regression from a suit of known samples, with no prior assumptions about physical behavior of the device or related media.
3. Look-up tables which define the conversion between a device space and a CIE color space at a series of coordinates within the color space, and interpolate the values for intermediate coordinates. The entries in a look-up table can be determined either by direct measurement or through a physical or numerical model.

No single device model gives can predict all the results from different sorts of device, thus a wide range of different models have been developed. Most device models are developed by measuring a sample of the colors on the media which is to be characterized in the beginning, and then defining a common relationship between

the two color spaces which are used to transform any color from one space to another.

Actually color transformations frequently include an element of two or even more of these methods. For example, a numerical method may be applied to define the relationship between printer and colorimetric values, with the exact dot areas to image found by a physical model, while the resulting function is applied to compute the entries in a look-up table of color. Then the resulting look-up table will be applied to show transformations of actual color image, as this will usually be more calculatingly efficient than computing the transformation on a pixel-by-pixel foundation. Alternatively a look-up table may be generated straightly from measurement data, in which case a lot of measurements will be required. The targets of device characterization can be outlined as follows:

Accuracy. The model should predict colors with smallest errors of the whole color space. The average color difference between predicted and measured colors should ideally be not larger than the noise performance within the system.

Visual acceptability. Discontinuities should not cause any artifact in the color model, and the errors distribution should not induce shifts in color attributes that are considered visually significant by observers.

Computational simplicity. This might be an important element where a device model is to run on personal computers or must be frequently recalculated to compensate for changes when media changes or device drift.

The minimum number of measurements. It is desirable to make the modeling process simpler, particularly where a numerical model has to be redefined because of different reproduction conditions when substrate is changed.

Analytic invertibility. Device models may need to compute both back up

transforms (e.g. from electronic device digit counts into another domain such as CIE colorimetry) and forward transforms (e.g. into colorant amounts). If a model is not invertible analytically, replacements are to use numeric methods to reverse the transform, or to determine the model from both directions. In both cases the forward and back up models are probable to have different errors, so that a color which is transformed from one color space to another and then back again will not have identical coordinates like the original [4].

2.2 Physical model

Physical model is based on physical properties of the device and the mixture of themselves. The color-mixing laws can be divided into two parts, additive and subtractive mixing. The technical terms additive and subtractive mixing traditionally have been used to distinguish between the colored lights mixing and the colorants mixing. The three additive primaries are red, green, and blue, while the three subtractive primaries are cyan, magenta, and yellow. Additive mixing primaries produce white, while subtractive mixing primaries produce black.

The typical example of additive color mixing is LED color mixing. In LED displays, three different types in the red, green, and blue of LEDs, are used. And then, we determine the chromaticity coordinates of the mixture of three separated emission bands. Suppose that the three emission bands have spectral power densities $P_1(\lambda)$, $P_2(\lambda)$, and $P_3(\lambda)$ with peak wavelengths of λ_1 , λ_2 , and λ_3 , respectively. We suppose that each emission band is much narrower than any other of the three color-matching functions. We further suppose that the three LED light sources have the chromaticity coordinates (x_1, y_1) , (x_2, y_2) , and (x_3, y_3) . Then the values of tristimulus are given by

$$X = \int_{\lambda} \bar{x}(\lambda)P_1(\lambda)d\lambda + \int_{\lambda} \bar{x}(\lambda)P_2(\lambda)d\lambda + \int_{\lambda} \bar{x}(\lambda)P_3(\lambda)d\lambda \approx \bar{x}(\lambda_1)P_1 + \bar{x}(\lambda_2)P_2 + \bar{x}(\lambda_3)P_3 \quad (2.1)$$

$$Y = \int_{\lambda} \bar{y}(\lambda)P_1(\lambda)d\lambda + \int_{\lambda} \bar{y}(\lambda)P_2(\lambda)d\lambda + \int_{\lambda} \bar{y}(\lambda)P_3(\lambda)d\lambda \approx \bar{y}(\lambda_1)P_1 + \bar{y}(\lambda_2)P_2 + \bar{y}(\lambda_3)P_3 \quad (2.2)$$

$$Z = \int_{\lambda} \bar{z}(\lambda)P_1(\lambda)d\lambda + \int_{\lambda} \bar{z}(\lambda)P_2(\lambda)d\lambda + \int_{\lambda} \bar{z}(\lambda)P_3(\lambda)d\lambda \approx \bar{z}(\lambda_1)P_1 + \bar{z}(\lambda_2)P_2 + \bar{z}(\lambda_3)P_3 \quad (2.3)$$

where P_1 , P_2 , and P_3 are the optical powers emitted by the three light sources.

Applying the abbreviations

$$L_1 = \bar{x}(\lambda_1)P_1 + \bar{y}(\lambda_1)P_1 + \bar{z}(\lambda_1)P_1 \quad (2.4)$$

$$L_2 = \bar{x}(\lambda_2)P_2 + \bar{y}(\lambda_2)P_2 + \bar{z}(\lambda_2)P_2 \quad (2.5)$$

$$L_3 = \bar{x}(\lambda_3)P_3 + \bar{y}(\lambda_3)P_3 + \bar{z}(\lambda_3)P_3 \quad (2.6)$$

the chromaticity coordinates of the color mixing light can be calculated from tristimulus values to yield

$$x = \frac{x_1L_1 + x_2L_2 + x_3L_3}{L_1 + L_2 + L_3} \quad (2.7)$$

$$y = \frac{y_1L_1 + y_2L_2 + y_3L_3}{L_1 + L_2 + L_3} \quad (2.8)$$

Hence, the chromaticity coordinate of the multi-element light is a linear combination of the separate chromaticity coordinates weighted by the L_i factors.

The color mixing principle in the chromaticity diagram is shown in Fig. 2-1. This diagram shows the two colors mixing with chromaticity coordinates (x_1, y_1) and (x_2, y_2) . And for the case of two colors, we set $L_3=P_3=0$. The mixed color will be located on the straight line of any point on the chromaticity coordinates of the two light sources. Thus, by mixing the two colors, any color (including white) located between the two chromaticity points can be created.

Fig. 2-1 also shows the mixing of three primary colors, located in the red, green, and blue locations of the chromaticity diagram. This three chromaticity points, connected by a dashed line, are general points of red, green, and blue LEDs. The area located inside the dash line, called the color gamut, shows all colors that can be generated by mixing the three colors red, green, and blue. For displays, the ability to create a great variety of colors is an important quality. It is a desirable that the color gamut provided by the three primary light sources is as large as possible to create displays able to show highly saturated colors.

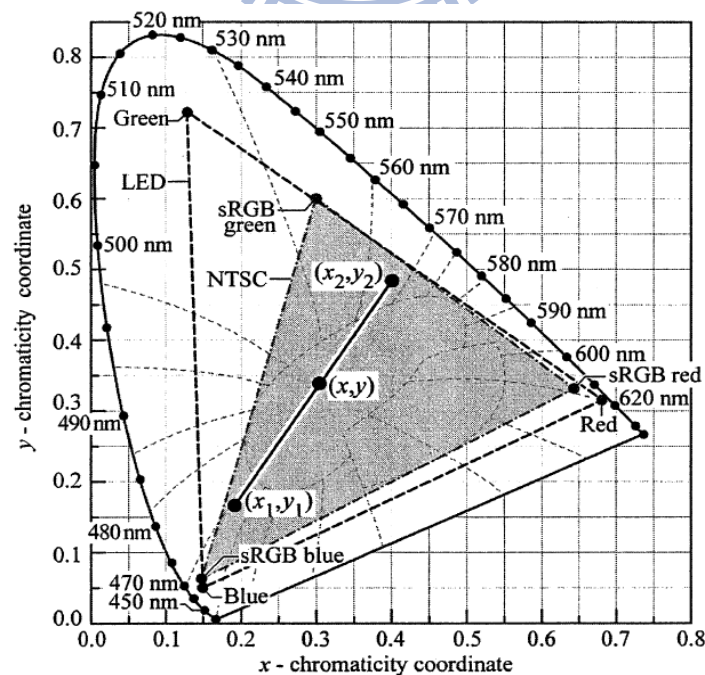


Fig. 2-1 Color gamut with three primary colors [7]

The color gamut shows the entire color range that can be created from a set of three primary sources. Color gamuts are polygons positioned within the perimeter of the chromaticity diagram. For example, the color gamut is a triangle with three primary colors, as shown in Fig. 2-1. All colors created by additive mixtures of the vertices (primary colors) of a gamut, are necessarily located within the gamut. The example of additive color mixing of LED is based on the independency (orthogonal) of three discrete emission bands. This phenomenon is shown as Fig. 2-2. Therefore, trichromatic white multi-LED can depend on its optical powers quantities of three primary colors to decide its chromaticity coordinates.

However, the LED additive color mixing is based on the emitting spectrum of light source. E-Papers are one sort of reflective display. So, if colorimetric characterization of e-Papers can be done by physical model, the reflectance spectrum should be measure first. Then, decide whether the reflectance spectrum of three primary colors has scalability or not. Scalability means that spectral quantity of normalized reflectance can multiply any constant to present their color properties. The hypothesis is that its three primary reflectance spectrum are independent.

There are many examples based on the subtractive principles, ex: Beer-Bouguer law for the homogeneous medium. However, the subtractive mixing would not be used in this thesis, the principles of subtractive mixing would not be talked.

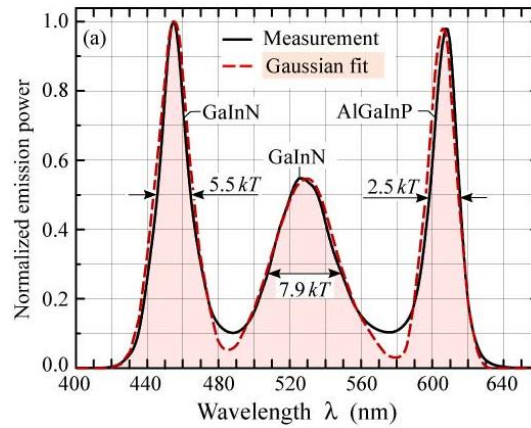


Fig. 2-2 Emission spectrum of trichromatic white multi-LED source with color temperature of 6500K (solid line) and gaussian fit (dashed line) [7]

2.3 Numerical model

To create a numerical model of the device space is first sampled colorimetrically so that the relationship between device values and tristimulus scalars is known for a given set of colors. The set is chosen so that the whole color space of device coordinates is depicted, and the known values that result are then used to derive a numerical model of the relationship between device space values and corresponding CIE color space scalars.

Polynomial regression is frequently used as mathematical tool in the numerical model. The polynomial regression is according to the assumption that the correlation between different color spaces can be approximated by a set of simultaneous equations. The schematic diagram of the regression method is represented in Fig. 2-3. Sample points of the source color space are selected and their color specifications of the destination color space are measured. A training set is a set of data used in various areas of information science to discover potentially predictive relationships. A testing set is a set of data used in various areas of information science to assess the strength and utility of a predictive relationship.

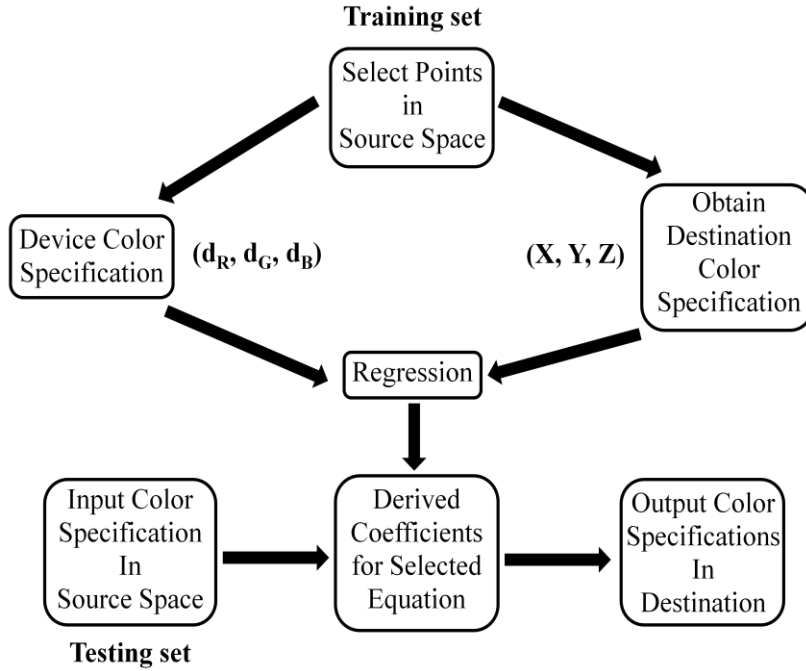


Fig. 2-3 Schematic diagram of the regression method

To link the source and destination color specifications, different levels of polynomial regression are used, as shown in Table 2-1. The general three-variable cubic expression is given in Eq. 2.9.

$$P_i(v) = a_{i0} + \sum_{j=1}^3 a_{ij} v_r + \sum_{j=4}^9 a_{ij} v_r v_s + \sum_{j=10}^{36} a_{ij} v_r v_s v_t \quad r, s, t=1, 2, \text{ or } 3 \quad (2.9)$$

A regression is used to select points with known color specifications for deriving the coefficients of the polynomial between source and destination spaces. The only necessity is that the number of selected points should be more than the number of polynomial terms which have to be calculated; otherwise, there will be no definite solutions to the simultaneous equations because there are more unknown variables than equations. By using derived coefficients, one can connect the source specifications to the simultaneous equations for computing the destination

specifications.

Table 2-1 The polynomials for color space conversion

$$1.P(R,G,B) = a_1R+a_2G+a_3B$$

$$2.P(R,G,B) = a_0+a_1R+a_2G+a_3B$$

$$3.P(R,G,B) = a_1R+a_2G+a_3B+a_4RG+a_5GB+a_6BR$$

$$4.P(R,G,B) = a_0+a_1R+a_2G+a_3B+a_4RG+a_5GB+a_6BR+a_{10}RGB$$

$$5.P(R,G,B) = a_1R+a_2G+a_3B+a_4RG+a_5GB+a_6BR+a_7R^2+a_8G^2+a_9B^2$$

$$6.P(R,G,B) = a_0+a_1R+a_2G+a_3B+a_4RG+a_5GB+a_6BR+a_7R^2+a_8G^2+a_9B^2+a_{10}RGB$$

$$7.P(R,G,B)=a_0+a_1R+a_2G+a_3B+a_4RG+a_5GB+a_6BR+a_7R^2+a_8G^2+a_9B^2+a_{10}RGB+a_{11}R^3+a_{12}G^3+a_{13}B^3$$

$$8.P(R,G,B) = a_0+a_1R+a_2G+a_3B+a_4RG+a_5GB+a_6BR+a_7R^2+a_8G^2+a_9B^2+a_{10}RGB+a_{11}R^3+a_{12}G^3+a_{13}B^3+a_{14}RG^2+a_{15}R^2G+a_{16}GB^2+a_{17}G^2B+a_{18}BR^2+a_{19}B^2R$$

(R, G, B) in Table 2-1 are digit counts of device color space, $P(R, G, B)$ is CIEXYZ values of destination color space. What the value of $P(R, G, B)$ is X, Y, or Z is depending on the coefficients representing a_x, a_y, a_z . The equation 1 of Table 2-1 is taken for an example to show what the value of $P(R, G, B)$ is X, Y, or Z is as follows,

$$X = P(R,G,B) = a_{1x}R+a_{2x}G+a_{3x}B \quad (2.10)$$

$$Y = P(R,G,B) = a_{1y}R+a_{2y}G+a_{3y}B \quad (2.11)$$

$$Z = P(R,G,B) = a_{1z}R + a_{2z}G + a_{3z}B \quad (2.12)$$

Polynomial regression is an application of the multiple linear regressions of m variables, where m is a number greater than the number of independent variables. The general approach of the linear regression with m variables is given as follows:

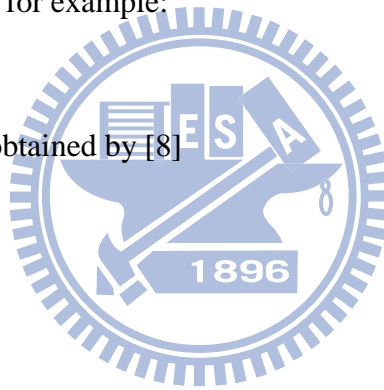
$$p_i = a_1u_{i1} + a_2u_{i2} + \dots + a_mu_{im} \quad (2.13)$$

For the application to the polynomial regression with three independent variables R, G, and B taken for example:

$$u_1=R, u_2=G, u_3=B$$

The coefficients are obtained by [8]

$$a=(UU')^{-1}(UP) \quad (2.14)$$



With n sets of inputs, U is a matrix of size $m \times n$, where m is the number of terms in the polynomial. U' is the transpose of U . The method above is also called least square method. Once the coefficients of regression methods are calculated, the chosen testing set would be substitute into these regression equations to testify the accuracy of numerical model. Numerical model with regression methods is ideal for transformation with a linear relationship. For nonlinear color space, this method does not guarantee uniform accuracy of the entire color space. In general, the accuracy improves as the number of terms in the equation increases [9, 10]. And another colorimetric characterization method in look-up table will be introduced below.

2.4 Look-up tables with interpolation

In color space transformation, the three-dimensional (3D) look-up table (LUT) with interpolation is a relatively new development. It includes three portions—packing (or partition), extraction (or find), and interpolation (or computation) [11]. The flow chart is shown the 3D LUT with interpolation consists of these three parts as Fig. 2-4.

Packing is a procedure that divides the source space domain and populates it with sample points to build up the lookup table. Generally, the table is built up by an equal-partition sampling along each axis of the source space as shown in Fig. 2-5(a). This will give n^3 lattice points and $(n - 1)^3$ cubes, where n is the number of levels. The benefit of this arrangement is that it implicitly provides the information about which cell is next to which. Hence, one only needs to store the starting point and the spacing for each axis. In general, a matrix of n^3 color patches at the lattice points of the source should be made, and the destination color specifications of these color patches are measured. The corresponding values from the source and destination spaces are listed into a lookup table. Non-lattice points are interpolated by utilizing the nearest lattice points. This is the step where the extraction executes a search to choose the lattice points necessary for calculating the destination spaces are listed into a lookup table. A well-packed space can make the search simpler. In an 8-bit integer setting, for example, if the axis is divided into 2^j equal partitions where j is an integer smaller than 8, and then the nearest lattice points are given in the most significant j bits (MSB_j) of the input color signals. That is to say, the input points is constrained in between the lattice points of $p(MSB_j)$ and $p(MSB_j + 1)$. This involves the operations of masking and shifting bits on computer, and these operations are faster than the comparison operation. For non-equally partitioned packing which is illustrated like

Fig. 2-5(b), a series of comparisons will be needed to confirm the locations of the nearest lattice points. It is required to further selection within the cubic lattice points. Depending on the interpolation technique used to count the color values of non-lattice points, we have the geometrical method.

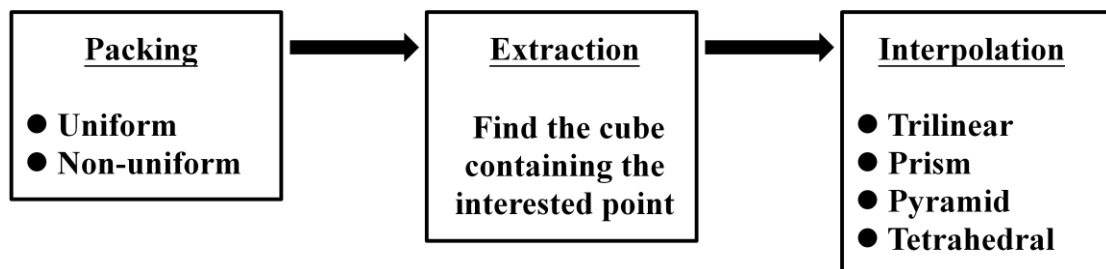


Fig. 2-4 Flow chart of 3D LUT

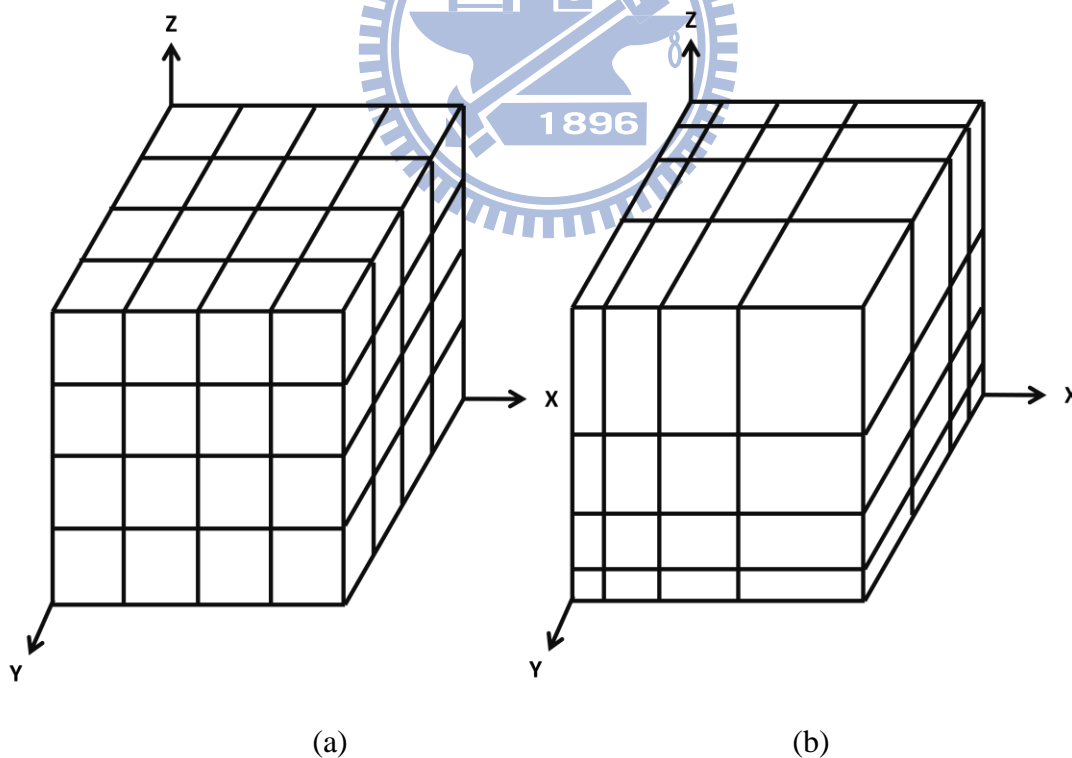


Fig. 2-5 (a) Equal-partition sampling

(b) Unequal-partition sampling of color space (XYZ)

2.4.1 Examples of 3-D interpolation

Here, we take a five-level lookup table to make a color transformation from RGB device space to CIELab color coordinates for example. The first step is to choose lattice points in the original RGB space with known color digit counts. A usual method is to divide the original space equally

R:	0.0	0.25	0.5	0.75	1.0
G:	0.0	0.25	0.5	0.75	1.0
B:	0.0	0.25	0.5	0.75	1.0
Eight-bit depth:	0	64	128	192	255

The second step is to make total of 125 lattice points with all combinations of R, G, and B levels. The third step is to extract. The extraction is to find the cube which contains the point (or color) of interest. For example, an input point p (5, 88, 160) has the device RGB values of R=5, G=88, B=160.

The point is bounded in the following ranges:

	lower range		point		upper range
R:	0	<	5	<	64
G:	64	<	88	<	128
B:	128	<	160	<	192

When the bounding box is determined, the eight vertices and their corresponding color specifications are extracted in the destination space. The final step is computation. Here, we have to choose 3-D geometrical interpolation methods. There are four common 3-D geometrical interpolation methods, including trilinear, prism, pyramid, and tetrahedral interpolation, respectively. Then, use one interpolation tool of these four methods to expand to full color space we want. The

examples of trilinear, prism, pyramid, and tetrahedral interpolation methods will be shown below.

2.4.2 Trilinear interpolation

Before we talk about trilinear interpolation, we have to introduce bilinear interpolation. In two dimensions, two variables $p(x, y)$ should be derived, and we have four known lattice points $p_{00}(x_0, y_0)$, $p_{01}(x_0, y_1)$, $p_{10}(x_1, y_0)$, $p_{11}(x_1, y_1)$. The figure of bilinear interpolation is shown as Fig. 2-6. The detail $p(x, y)$ formula is like this:

$$p(x, y) = p_{00} + [(x - x_0) / (x_1 - x_0)](p_{10} - p_{00}) + [(y - y_0) / (y_1 - y_0)](p_{01} - p_{00}) + [(x - x_0) / (x_1 - x_0)][(y - y_0) / (y_1 - y_0)](p_{11} - p_{01} - p_{10} + p_{00}) \quad (2.15)$$

And then, we can use this bilinear interpolation method to expand to trilinear interpolation (as Fig. 2-7).

$$p(x, y, z) = c_0 + c_1 \Delta x + c_2 \Delta y + c_3 \Delta z + c_4 \Delta x \Delta y + c_5 \Delta x \Delta z + c_6 \Delta y \Delta z + c_7 \Delta x \Delta y \Delta z \quad (2.16)$$

$$\Delta x = x - x_0$$

$$\Delta y = y - y_0$$

$$\Delta z = z - z_0$$

$$c_0 = p_{000}$$

$$c_1 = (p_{100} - p_{000}) / (x_1 - x_0)$$

$$c_2 = (p_{010} - p_{000}) / (y_1 - y_0)$$

$$c_3 = (p_{001} - p_{000}) / (z_1 - z_0)$$

$$c_4 = (p_{110} - p_{010} - p_{100} + p_{000}) / [(x_1 - x_0)(y_1 - y_0)]$$

$$c_5 = (p_{101} - p_{001} - p_{100} + p_{000}) / [(x_1 - x_0)(z_1 - z_0)]$$

$$c_6 = (p_{011} - p_{001} - p_{010} + p_{000}) / [(y_1 - y_0)(z_1 - z_0)]$$

$$c_7 = (p_{111} - p_{011} - p_{101} - p_{110} + p_{100} + p_{001} + p_{010} - p_{000}) / [(x_1 - x_0)(y_1 - y_0)(z_1 - z_0)]$$

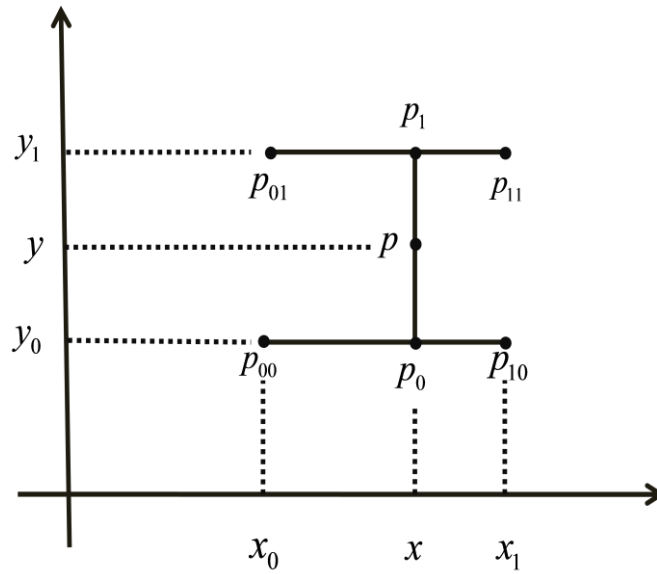


Fig. 2-6 Bilinear interpolation [12]

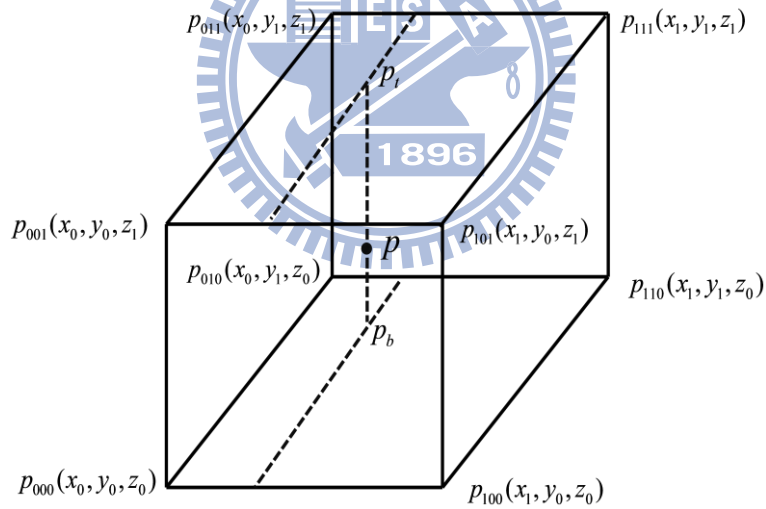


Fig. 2-7 Trilinear interpolation [12]

So, $p(x, y, z)$ could be found by this trilinear interpolation formula. This method requires ten multiplications and seven additions, with thirteen pre-computed coefficients stored at each node.

2.4.3 Prism interpolation

If a cube is cut diagonally into two halves as shown in Fig. 2-8, a cube gets two prism shapes. For locating the point of interest, a search mechanism is needed. Owing to these two symmetric structures in the cube, a simple inequality comparison is sufficient to determine the location: if $\Delta x > \Delta y$, then the point is in prism 1; otherwise the point is in prism 2. For $\Delta x = \Delta y$, the point is located on the diagonal plane, then either prism can be used for interpolation. Each equation has six terms and uses six vertices of the prism to compute. This method requires eight multiplications and five additions with seven coefficients at each node.

$$\Delta x > \Delta y$$

$$p(x, y, z) = p_{000} + (p_{100} - p_{000})\Delta x / (x_1 - x_0) + (p_{110} - p_{100})\Delta y / (y_1 - y_0) + (p_{001} - p_{000})\Delta z / (z_1 - z_0) + (p_{101} - p_{001} - p_{100} + p_{000})\Delta x\Delta z / [(x_1 - x_0)(z_1 - z_0)] + (p_{111} - p_{101} - p_{110} + p_{100})\Delta y\Delta z / [(y_1 - y_0)(z_1 - z_0)]$$

$$\Delta y > \Delta x$$

$$p(x, y, z) = p_{000} + (p_{110} - p_{010})\Delta x / (x_1 - x_0) + (p_{010} - p_{000})\Delta y / (y_1 - y_0) + (p_{001} - p_{000})\Delta z / (z_1 - z_0) + (p_{111} - p_{011} - p_{110} + p_{010})\Delta x\Delta z / [(x_1 - x_0)(z_1 - z_0)] + (p_{101} - p_{001} - p_{100} + p_{000})\Delta y\Delta z / [(y_1 - y_0)(z_1 - z_0)] \quad (2.17)$$

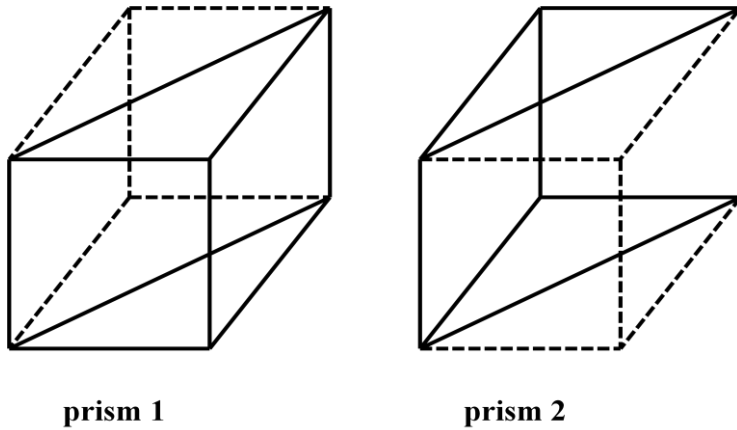


Fig. 2-8 Prism interpolation [12]

2.4.4 Pyramid interpolation

For pyramid interpolation, the cube is cut into three parts; each part takes a face as the pyramid base possessing its corners linked to a vertex in the opposite side as the apex (as shown in Fig. 2-9). For locating the interpolation point, the search mechanism given in Table 2-2 is used. Each equation has five terms and uses five vertices of the pyramid for computation. This method requires seven multiplications and four additions with five coefficients at each node.

Table 2-2 The inequality relationships and the coefficients for pyramid interpolation

Pyramid	Test	c_1	c_2	c_3	c_4
1	$\Delta y > \Delta x,$ $\Delta z > \Delta x$	$p_{111} - p_{011}$	$p_{010} - p_{000}$	$p_{001} - p_{000}$	$p_{011} - p_{001} - p_{010} + p_{000}$
2	$\Delta x > \Delta y,$ $\Delta z > \Delta y$	$p_{100} - p_{000}$	$p_{111} - p_{101}$	$p_{001} - p_{000}$	$p_{101} - p_{001} - p_{100} + p_{000}$
3	$\Delta y > \Delta z,$ $\Delta x > \Delta z$	$p_{100} - p_{000}$	$p_{010} - p_{000}$	$p_{111} - p_{110}$	$p_{110} - p_{100} - p_{010} + p_{000}$

Pyramid 1:

$$p(x, y, z) = p_{000} + c_1 \Delta x / (x_1 - x_0) + c_2 \Delta y / (y_1 - y_0) + c_3 \Delta z / (z_1 - z_0) + c_4 \Delta y \Delta z / [(y_1 - y_0)(z_1 - z_0)]$$

Pyramid 2:

$$p(x, y, z) = p_{000} + c_1 \Delta x / (x_1 - x_0) + c_2 \Delta y / (y_1 - y_0) + c_3 \Delta z / (z_1 - z_0) + c_4 \Delta x \Delta z / [(x_1 - x_0)(z_1 - z_0)]$$

Pyramid 3:

$$p(x, y, z) = p_{000} + c_1 \Delta x / (x_1 - x_0) + c_2 \Delta y / (y_1 - y_0) + c_3 \Delta z / (z_1 - z_0) + c_4 \Delta x \Delta y / [(x_1 - x_0)(y_1 - y_0)] \quad (2.18)$$

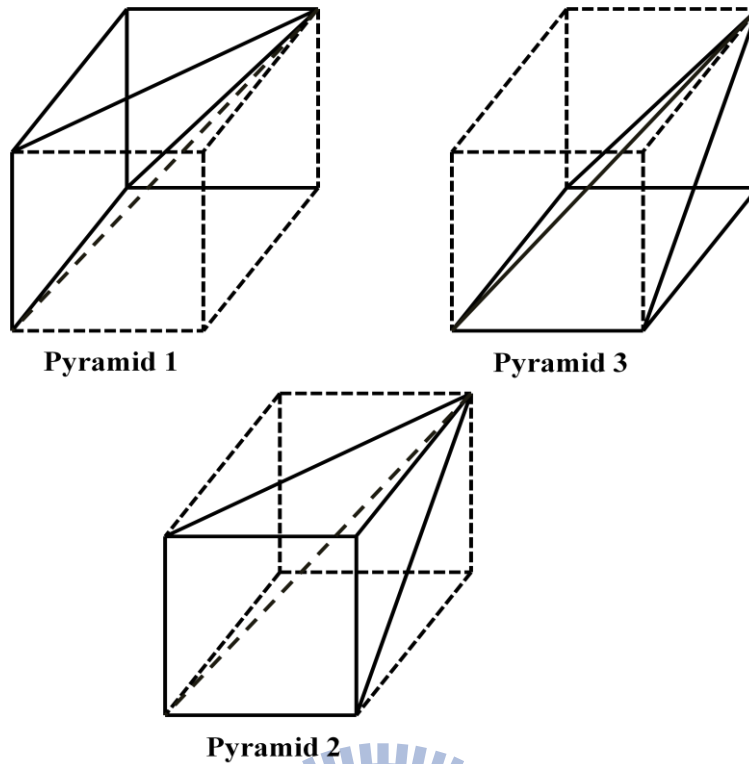


Fig. 2-9 Pyramid interpolation [12]

2.4.5 Tetrahedral interpolation

We will present the details of an efficient and accurate method for color interpolation which is frequently used in practical applications. There are many methods for splitting a cube into many tetrahedra, and no matter what methods we using, we should follow these principles below:

1. Try to use all vertices of a cube, and the using frequency is as many as well.
2. The cube may be all filled with tetrahedron.
3. The linking surfaces of tetrahedron should be complete, in other words, the area of linking surfaces should be the same.

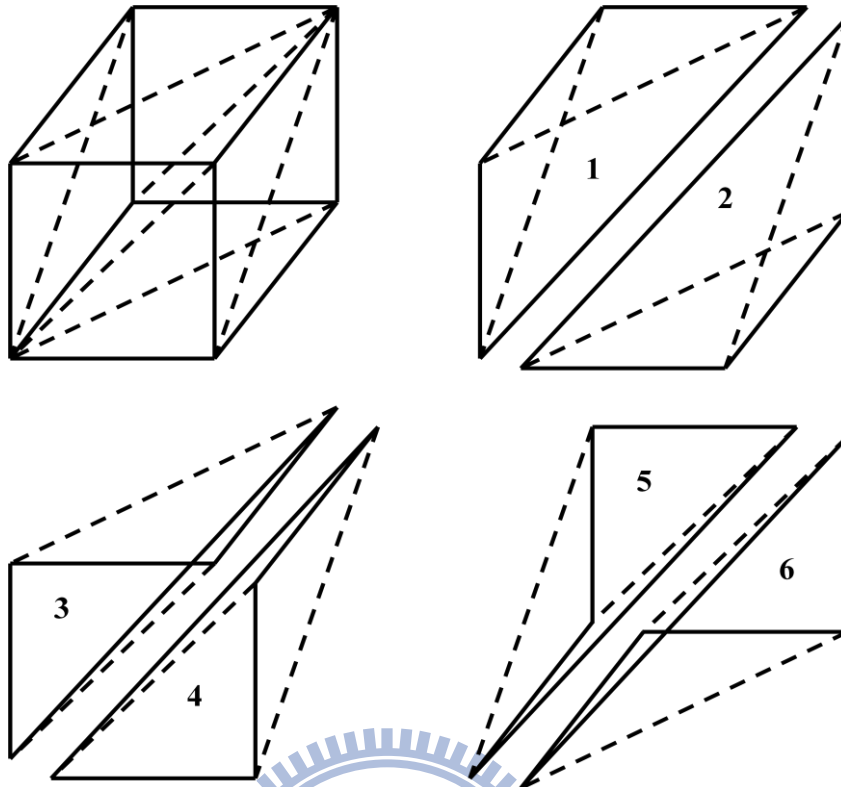


Fig. 2-10 Tetrahedral interpolation

According to these principles and computation, the method of diagonal extraction in tetrahedral interpolation is usually used. As shown in Fig. 2-10, the tetrahedral interpolation [13] cuts a cube into six tetrahedrons; everyone has a triangle base.

The problem is described in Fig. 2-11. Given a tetrahedron in an (r, g, b) digit count color space and its corresponding tetrahedron in another color space (X, Y, Z) , for any point in (X, Y, Z) space, determine whether the point is inside the tetrahedron or not, and if yes, determine its corresponding coordinates in the (r, g, b) color space. To solve these problems, it is convenient to take one of the four vertices (see Fig. 2-12), say vertex P_0 , as the origin and regard the edges from P_0 to the other three vertices P_1, P_2 , and P_3 , as vectors, $\overline{P_0P_1}$, $\overline{P_0P_2}$ and $\overline{P_0P_3}$:

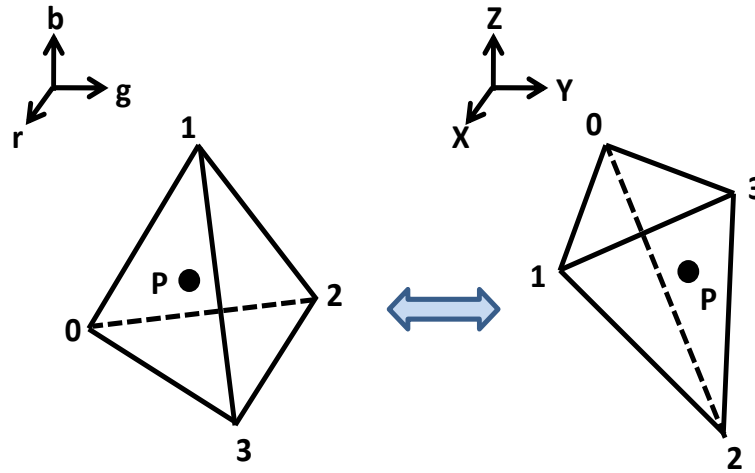


Fig. 2-11 The tetrahedral interpolation problem

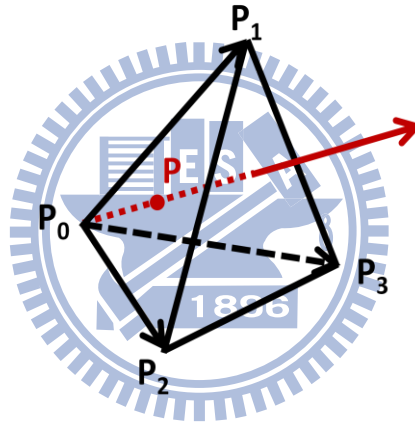


Fig. 2-12 The convex inclusion problem [14]

How to determine if a point is inside a given tetrahedron? We set $\overline{P_0P_1}$, $\overline{P_0P_2}$ and $\overline{P_0P_3}$ three linearly independent vectors, then for any point P in the space, the vector $\overline{P_0P}$ can be expressed as a linear sum of the three vectors $\overline{P_0P_1}$, $\overline{P_0P_2}$, and $\overline{P_0P_3}$:

$$\overline{P_0P} = \alpha \overline{P_0P_1} + \beta \overline{P_0P_2} + \gamma \overline{P_0P_3} \quad (2.19)$$

$$\begin{bmatrix} r_p - r_0 \\ g_p - g_0 \\ b_p - b_0 \end{bmatrix} = \begin{bmatrix} r_1 - r_0 & r_2 - r_0 & r_3 - r_0 \\ g_1 - g_0 & g_2 - g_0 & g_3 - g_0 \\ b_1 - b_0 & b_2 - b_0 & b_3 - b_0 \end{bmatrix} \begin{bmatrix} \alpha \\ \beta \\ \gamma \end{bmatrix} \quad (2.20)$$

Point P is inside the tetrahedron only if $\alpha \geq 0, \beta \geq 0, \gamma \geq 0$, and $\alpha + \beta + \gamma \leq 1$,

where

$$\begin{bmatrix} \alpha \\ \beta \\ \gamma \end{bmatrix} = \begin{bmatrix} r_1 - r_0 & r_2 - r_0 & r_3 - r_0 \\ g_1 - g_0 & g_2 - g_0 & g_3 - g_0 \\ b_1 - b_0 & b_2 - b_0 & b_3 - b_0 \end{bmatrix}^{-1} \begin{bmatrix} r_p - r_0 \\ g_p - g_0 \\ b_p - b_0 \end{bmatrix} \quad (2.21)$$

The above conditions can be proved as depicted below:

1. P_0 and P are on the same side of the plane $P_1P_2P_3 \leftrightarrow \alpha + \beta + \gamma \leq 1$.
2. P_1 and P are on the same side of the plane $P_0P_2P_3 \leftrightarrow \alpha \geq 0$.
3. P_2 and P are on the same side of the plane $P_1P_0P_3 \leftrightarrow \beta \geq 0$.
4. P_3 and P are on the same side of the plane $P_1P_2P_0 \leftrightarrow \gamma \geq 0$.

What are the (r, g, b) coordinates of an inner point P ? When P is inside the tetrahedron, its (r, g, b) coordinates can be determined from the decided four vertices by:

$$\begin{bmatrix} X_p \\ Y_p \\ Z_p \end{bmatrix} = \begin{bmatrix} X_1 - X_0 & X_2 - X_0 & X_3 - X_0 \\ Y_1 - Y_0 & Y_2 - Y_0 & Y_3 - Y_0 \\ Z_1 - Z_0 & Z_2 - Z_0 & Z_3 - Z_0 \end{bmatrix} \begin{bmatrix} \alpha \\ \beta \\ \gamma \end{bmatrix} + \begin{bmatrix} X_0 \\ Y_0 \\ Z_0 \end{bmatrix} \quad (2.22)$$

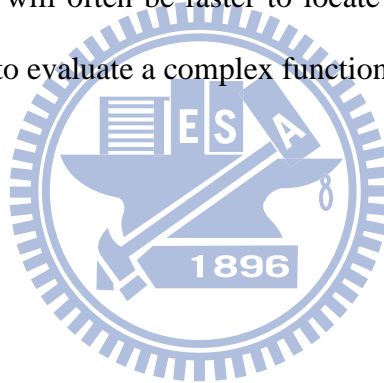
The general formula of eq. (2.22) is illustrated below:

$$\begin{aligned}
X_p &= X_0 + \alpha(X_1 - X_0) + \beta(X_2 - X_0) + \gamma(X_3 - X_0) \\
Y_p &= Y_0 + \alpha(Y_1 - Y_0) + \beta(Y_2 - Y_0) + \gamma(Y_3 - Y_0) \\
Z_p &= Z_0 + \alpha(Z_1 - Z_0) + \beta(Z_2 - Z_0) + \gamma(Z_3 - Z_0)
\end{aligned}
\tag{2.23}$$

This method requires six multiplications and three additions with three coefficients at each node.

2.4.6 Applications of 3D interpolation

Many applications of 3D interpolation in printer, monitor, and scanner calibration have been published in the literature. LUTs are applied where two domains are not easily related, as it will often be faster to locate the values and perform any interpolation required than to evaluate a complex function.



Chapter 3

Colorimetric Characterization on ChLCD

3.1 Introduction of cholesteric liquid crystal

The chiral nematic liquid crystal is also named cholesteric liquid crystal (ChLC). Unlike the traditional nematic liquid crystal, ChLC includes a chiral center in the nematic mesogenic molecules. If the twisting power for chirality is strong enough, ChLC material is integrated when the nematic liquid crystal and chiral dopant are mixed. The chirality generates an intermolecular force that results in a twist between each layer. In different cholesteric liquid crystal systems, the period of the helical pitch varies by a wide range. For the long pitch (low concentration chirality) $P \gg \lambda$ (where λ is the wavelength of light), the light propagation parallel to the helix axis may be characterized by a superposition of two eigenwaves having electric field vectors parallel and perpendicular to the director. For short pitch (high concentration chirality), the eigenwaves may become elliptical, and may be circular in the limiting case. The ChLC molecule structure is shown in Fig. 3-1.

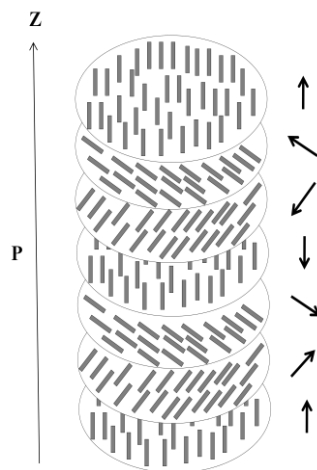


Fig. 3-1 ChLC molecule structure, where P is the helical pitch with ChLC molecule rotating 360° perpendicular to Z-axis

3.1.1 Optical characteristics in different textures

ChLCs are simple to change its texture by adding electric or magnetic field. Again, we add electric field instead of magnetic field in common cholesteric liquid crystal devices. When an electric field applied to the ChLCs cell, a texture transition happens to minimize the free energy system. The texture transition is strongly associated with dielectric anisotropic $\Delta\epsilon$, field amplitude, alignment layer, and the frequency of the external field. The typically operating modes which are used in common cholesteric liquid crystal display are described as Fig. 3-2.

When the ChLCs operate in the planar texture at zero field, the helical axis is perpendicular to the cell surface as shown in Fig. 3-2(a). It reflects the selective reflection light by Bragg diffraction. The texture would be changed into the focal conic texture when applied electric field $V \geq V_{th}$ (threshold voltage). In the focal conic texture, the helical axis is more or less parallel to the surface as shown in Fig. 3-2 (b). Incident light is diffracted or scattered in the forward direction and the material in this state has less reflective color appearance. And then, the high-voltage pulses can transform the liquid crystal from the focal conic texture to homeotropic texture (as Fig. 3-2 (c)). If the applied voltage is switched to a medium bias level, the liquid crystal relaxes to focal conic texture; if the applied voltage is switched to a low bias level, the liquid crystal relaxes to planar texture. The channels of switching between three textures [15] are illustrated in Fig. 3-3. It is noted that ChLCs can exhibit two stable textures at zero field. One of them is the planar texture, and the other is the focal conic texture. So the ChLCs material has the bistable property that is an advantage for display technology.

When the dielectric anisotropy $\Delta\epsilon > 0$:



Fig. 3-2 Schematic diagram for different textures of the ChLCs

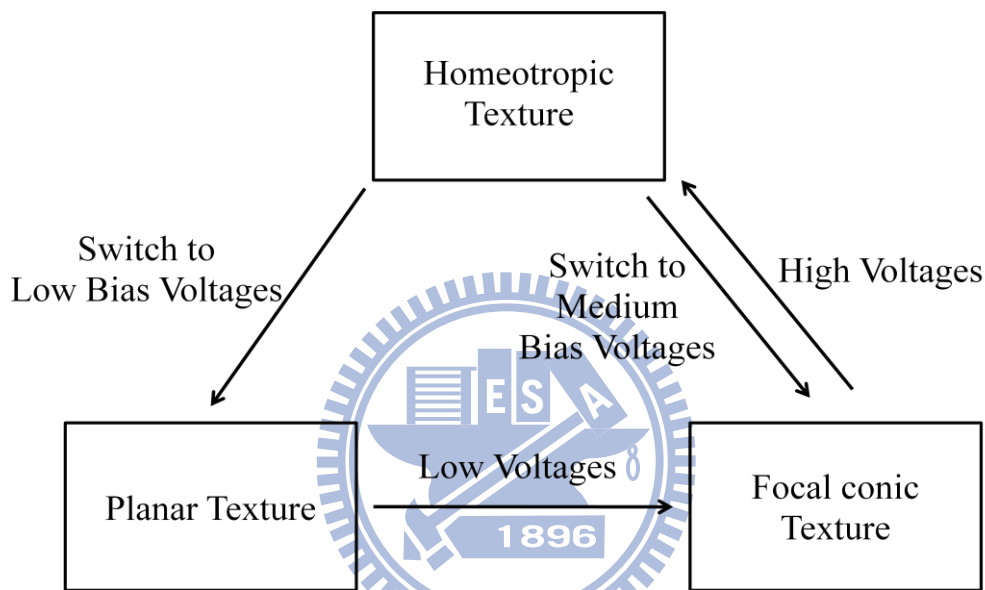


Fig. 3-3 Possible field-induced texture transition channels in ChLCs

3.1.2 Gray scale property of cholesteric liquid crystals

ChLCs exhibit gray scale property owing to their multi-domain structure when the planar texture and the focal conic texture are appeared simultaneously. From the imperfect planar texture, some domains can be switched into the focal conic texture if the threshold voltage is exceeded. The reflective color luminance will be decreased. The figure of the gray scale states of a ChLCs display is illustrated in Fig. 3-4. From left to right, the states are achieved by applying voltage pulses with increasing amplitude.

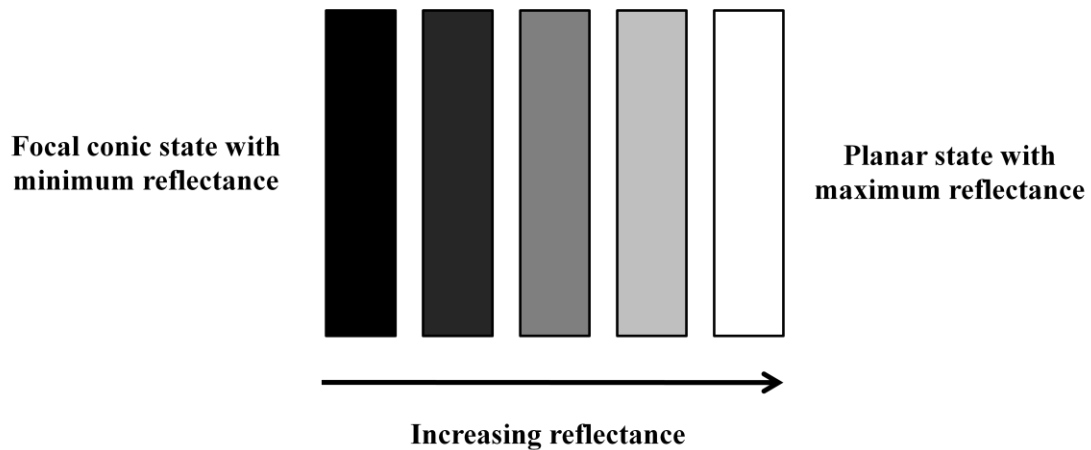


Fig. 3-4 The gray scale states of a ChLCDs display [16]

3.2 Physical mechanism of three-layers-stacked ChLCD

The three-layers-stacked ChLCD which is as implied by the name is composed of three layers. The top layer selectively reflects blue light, the center layer reflects green light while the bottom layer selectively reflects red light. The fundamental structure is shown as Fig. 3-5. And the stacking structure using additive color approach.

For example, blue color is exhibited with the top layer which operates in the reflective texture and another two layers operate in focal conic texture. Another two colors are vice versa [17]. When the liquid crystal is in the focal conic texture, many domains still have the helical axes perpendicular to the surface of the cells because of the strong homogeneous surface anchoring, and the reflection is relatively high [18]. So, although another two layers operate in the focal conic texture, the diffusion light from these layers also influence the colors we want to exhibit.

When the helical structure is operated in planar texture (as illustrated in Fig. 3-6), normally incident white light is decomposed into right and left circular parts

with one part reflected and the other transmitted. So, that is why reflectivity of the panel cannot be behind 50%.

A question comes out that—why the layer sequence is BGR, as shown in Fig. 3-5? The key point is depending on the reflectivity of each layer. Because the reflectivity is highest in blue-color state, three-layers-stacked ChLCD is made in this type. ‘The reflectance of the blue layer alone is 37% while the yellow reflectance is 30% [19] can prove this actuality. Here, Fig. 3-7 is the spectral reflection of three-layers-stacked ChLCD (FLEPia) under diffuse illumination. The spectral reflectivity of FLEPia would be decided whether it has scalability or not in chapter 4.

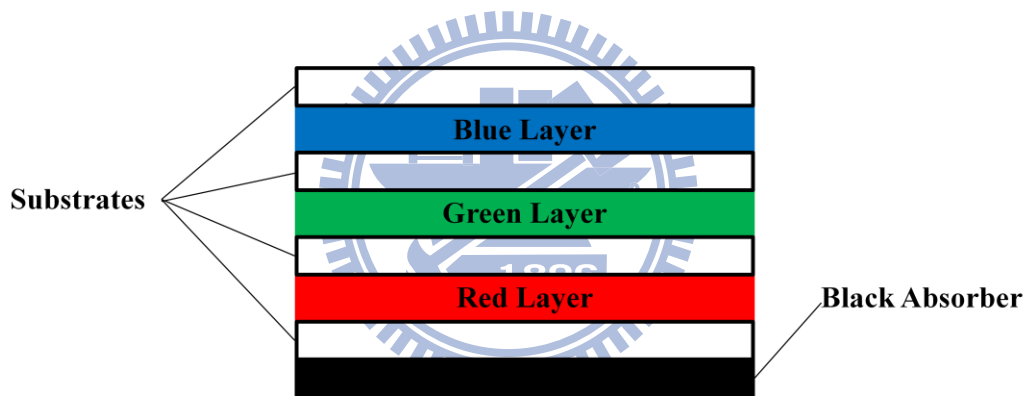


Fig. 3-5 A structure of three-layers-stacked ChLCD [20]

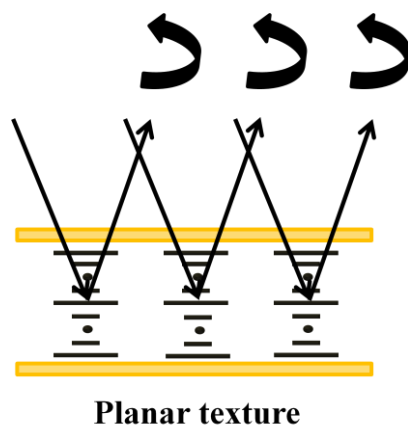


Fig. 3-6 Schematic illustration of the planar texture

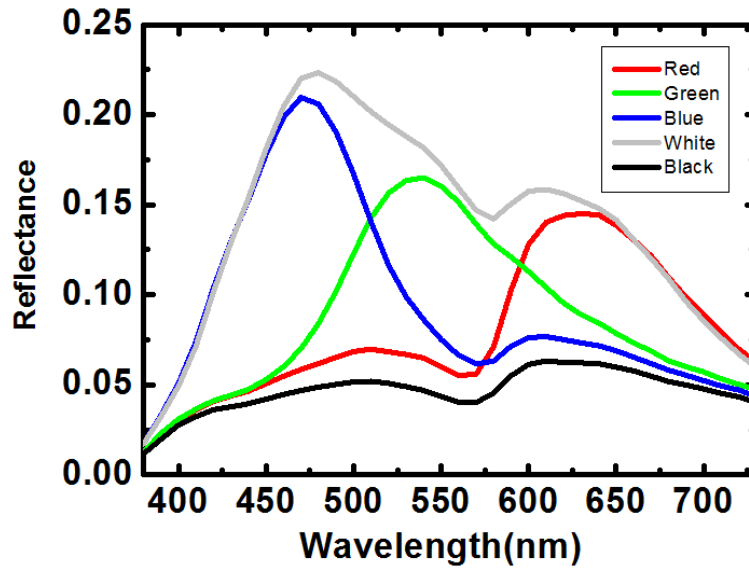


Fig. 3-7 Reflection spectrum of three-layers-stacked ChLCD (FLEPia)

3.3 Numerical method

In principle, the polynomial order can be up to $n-1$ (where n is the number of discrete samples), although since each additional order adds a possible bend to the function (such bends being known as local maxima or minima, or relative extrema) it is desirable to keep the polynomial order as low as possible. However, how many numbers of polynomial terms are suitable for our device. So, here a flow chart is presented how the suitable polynomial term is chosen as Fig. 3-8.

At first, the measured training sets are a set of nine-level, unequally spaced lattice points (729 points) which is from $9 \times 9 \times 9$ LUT talked in chapter 4 in the RGB space. Secondly, the measured training set may be substitute into regression equations. The predicting CIEXYZ values of these training set will be computed. Why the color differences of training sets were calculated is because that the polynomial regression computed from training sets is only the approximate form. We can examine the average color differences of training sets to determine whether this polynomial equation reaches our criterion or not. If the ΔE_{00_avg} between predicting and measured

training sets is behind 1, the polynomial term will be increased to 20 terms at most. Afterward, the CIEDE2000 color differences between the predicting and measured CIEXYZ values of testing samples will be calculated. If ΔE_{00_avg} between them is not below 1, the polynomial term will be also increased to 20 terms at most. Finally, whatever the ΔE_{00_avg} of training set and testing set in 20 terms polynomial are below 1 or not, the terms would not be increased anymore. Provided that the order of polynomials rises up to fourth order, the amounts of polynomial terms would increase to 60 terms mostly. This may cause calculating efficiency to drop. Therefore, polynomial of 20 terms is the most terms to be used.

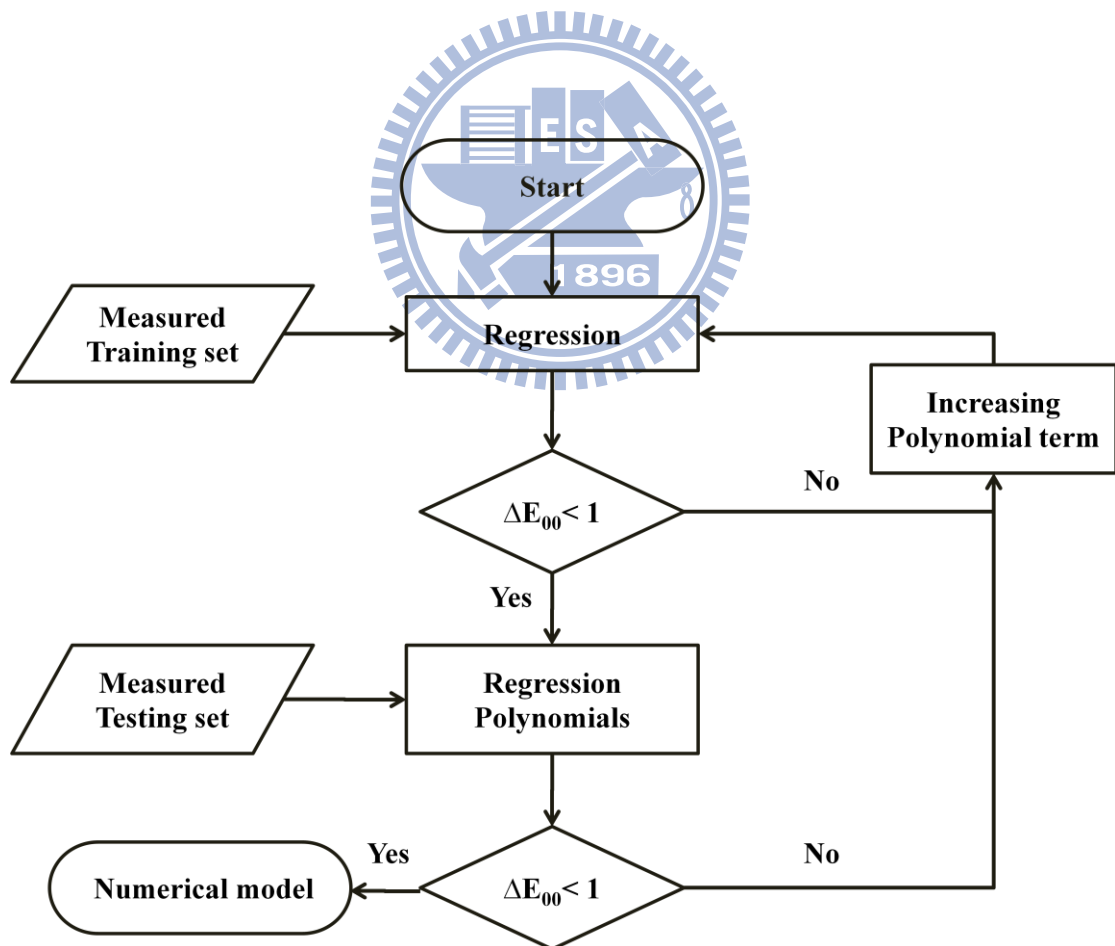
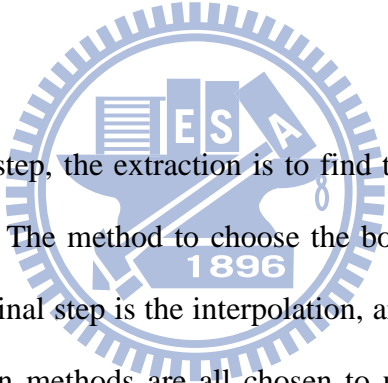


Fig. 3-8 Flow chart to determine coefficients and polynomial terms

3.4 Look-up table with interpolation

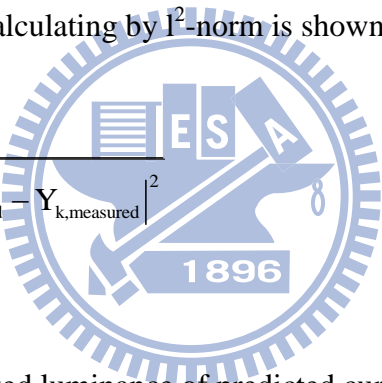
The first step here used to characterize three-layers-stacked ChLCD is non-uniform packing because its gamma curve is nonlinear. This reason is explained as Fig. 3-9, the gamma curve in green channel of Fujitsu FLEPia is very nonlinear. This form of LUT is very different from standard way of implementing LUT; in other words, the source color space is equally divided with respect to the sampling rate. This may cause an irregular and uneven destination space for those color conversions which are nonlinear. Many techniques have been offered to work on the non-uniform color space [21]. For this packing, each cube subcell will be replaced by rectangular one. The lattice points are selected using the gamma curve of RGB with respect to the normalized luminance.



When in the second step, the extraction is to find the cube which contains the point (or color) of interest. The method to choose the bounding box is like the way depicted in chapter 2. The final step is the interpolation, and trilinear, prism, pyramid, and tetrahedral interpolation methods are all chosen to use to interpolate full color space in ChLCD. Here, a flow chart is presented how the suitable packing number is chosen as Fig. 3-10.

At first, the gamma curves with respective R, G, B channel of Fujitsu FLEPia would be decided if its color conversion is linear. Secondly, if its color conversion is linear, its packing would be uniform; if its color conversion is nonlinear. The result showed that its packing would be non-uniform. Then, and the vertices of a cube for interpolation would be found by extraction. Finally, the value inside the polygon within a cube would be calculated by these four different geometrical interpolation methods, and the ΔE_{00_avg} between the predicted values by interpolation and the

measured values would be computed. If the average value is behind one, the packing number would be increased until the $\Delta E_{00_avg.}$ is below one. Finally, if the $\Delta E_{00_avg.}$ is below 1, it should be an adequate LUT. Fig. 3-9 is illustrated the gamma curve in only green channel of Fujitsu FLEPia for representative. The figure is proved that the gamma curve of Fujitsu FLEPia is very nonlinear. So, the chosen packing is non-uniform. Cubic of 3, 5, 7, and 9 non-uniform packing is chosen. And then, how the packing points are selected? The 0, 255 digit count is the necessary points. Another packing points is picked by the error calculating by l^2 -norm which is lowest between the gamma curve of Fujitsu FLEPia and the curve of packing points depend on piecewise linear method. The l^2 -norm is also known as Euclidean norm. The equation form of the error calculating by l^2 -norm is shown as Eq. (3.1).



$$|Y| = \sqrt{\sum_{k=0,4,8,\dots}^{255} |Y_{k,predicted} - Y_{k,measured}|^2} \quad (3.1)$$

$Y_{k, predicted}$ = normalized luminance of predicted curve of packing points with green channel depend on piecewise linear method

$Y_{k, measured}$ = normalized luminance of Fujitsu FLEPia with green channel

Finally, follow the methods above, the $\Delta E_{00_avg.}$ can be calculated.

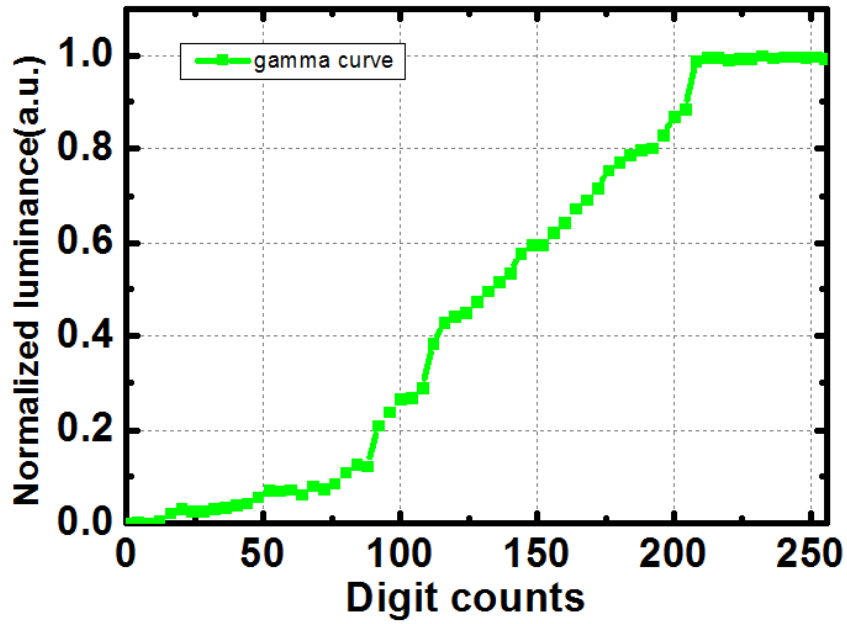


Fig. 3-9 The gamma curve in green channel of Fujitsu FLEPiA

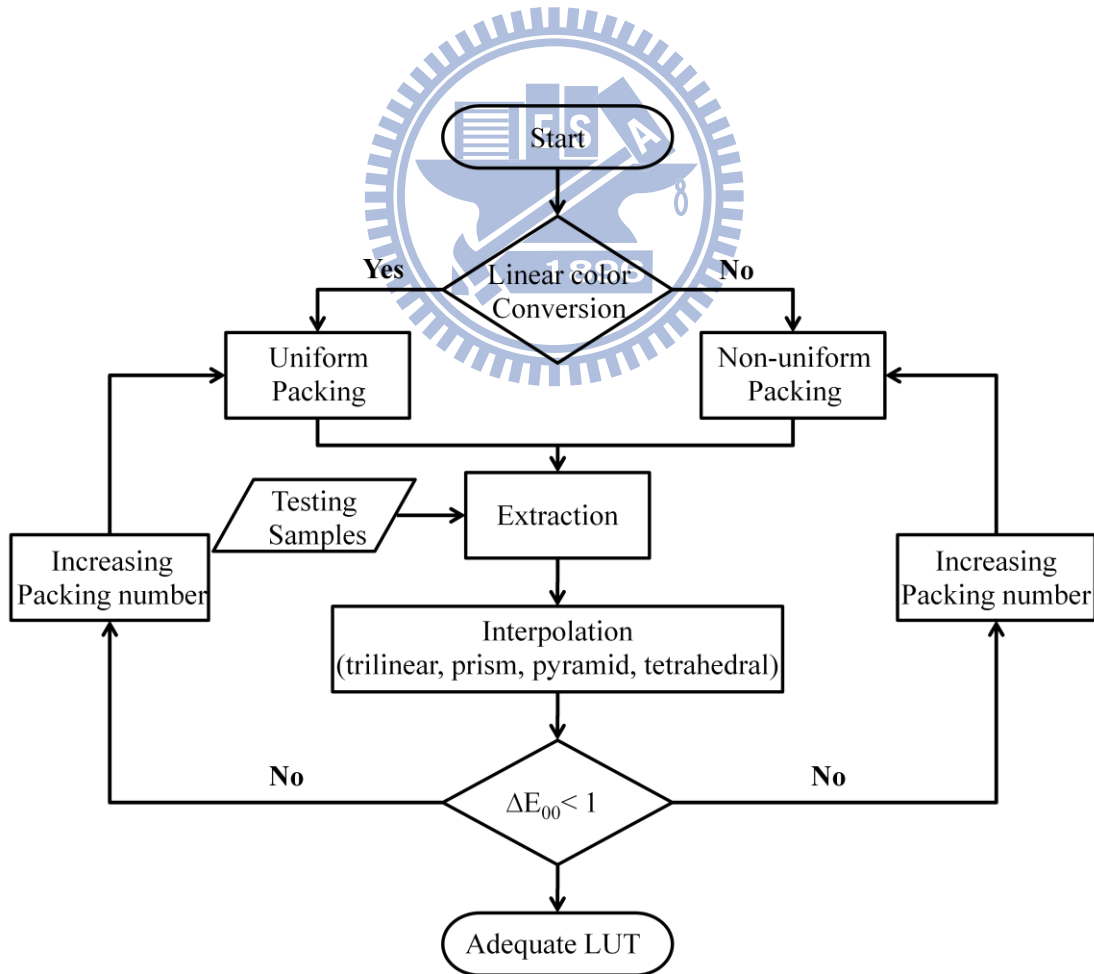


Fig. 3-10 Flow chart to choose numbers of packing

Chapter 4

Experiment and Verification

4.1 Experimental platform

For verifying color differences between the measurement data and numerical model or LUT, the stable experimental testing platform must be set up. The main two conditions of this experimental platform are: (a) full color three-layers-stacked ChLCD; (b) spectrophotometer to measure any optical physical quantity. The three-layers-stacked cholesteric liquid crystal display for experiment was Fujitsu FLEPia [22], and the spectrophotometer was x-rite i1 pro [23]. The specifications of the i1 Pro hardware device is as Table 4-1.

Table 4-1 Specifications of i1 Pro

Optical resolution	10nm
Physical sampling interval	3.5nm
Spectral data	Range: 380 ... 730 nm in 10nm steps
Measurement aperture	4.5mm diameter
Measurement geometry	45°/0° ring illumination optics, DIN 5033
Light source	Gas filled tungsten (Type A)

According to the specification, the average color difference of i1 Pro is 0.4 of ΔE^*_{94} , which is small enough to be used to measure the color performance. The specifications of Fujitsu FLEPia are summarized in Table 4-2.

Table 4-2 Specifications of Fujitsu FLEPia

Size	158 x 240 x 12.5 mm
Display	8 inch
Resolution	768 x 1024 pixels
Number of Displayable Colors	260,000 colors (64*64*64)

The experimental condition is shown as Fig. 4-1, and Fig. 4-2 is the practical platform setup during our experiment. The measurement geometry is $45^{\circ}/0^{\circ}$ ring illumination optics with gas filled tungsten (Type A) light source. The experiments were done in the darkroom. Fig. 4-3 is the flow chart of experiment. The computer was sent digital values to simulator which is Matlab program to control any color in Fujitsu FLEPia. And x-rite i1 pro was use to measure CIEXYZ of Fujitsu FLEPia.

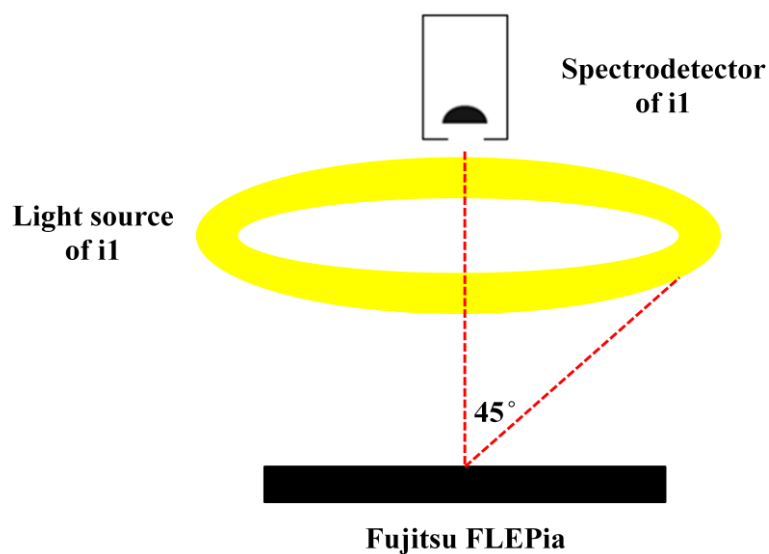


Fig. 4-1 Experimental condition figure



Fig. 4-2 Real construction figure of experiment

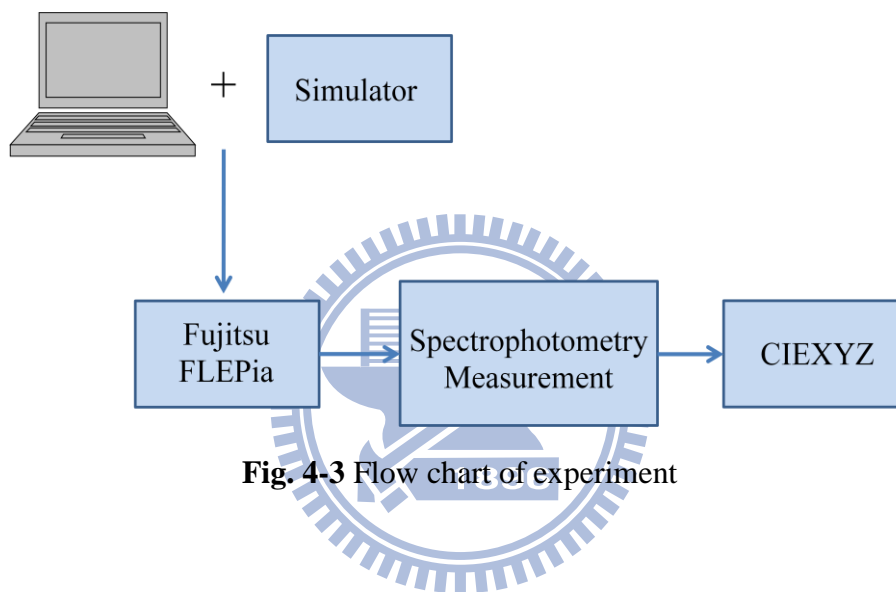


Fig. 4-3 Flow chart of experiment

4.2 Examination of performance in Fujitsu FLEPia

At first, the luminance of gray level and independent red, green, and blue color of 256 digit counts were measured as illustrated in Fig. 4-4. From this figure, these four gamma curves are not smooth enough to only utilize a simply analytical formula to represent their color performance, and each R, G, B curve does not overlap each other. Therefore, the characteristic curves cannot use only one fitting curve to represent them. Then, each X, Y, and Z value of green channel in Fujitsu FLEPia were also measured to test whether the normalized luminance values can represent three X, Y, and Z values or not.

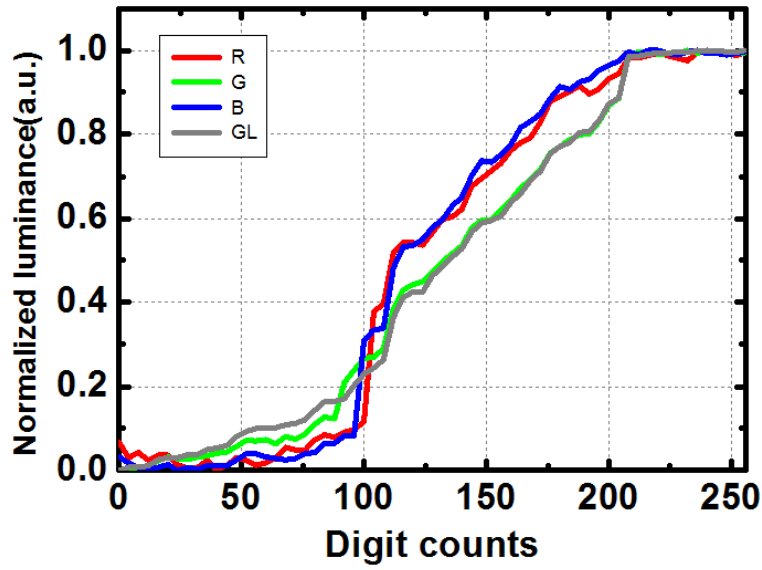


Fig. 4-4 Normalized luminance in 256 digit count of three independent channel and gray level

The figure of green channel each normalized X, Y, and Z value is shown as Fig. 4-5. Obviously, the normalized luminance curve of green channel cannot cover another two X, Z curve.

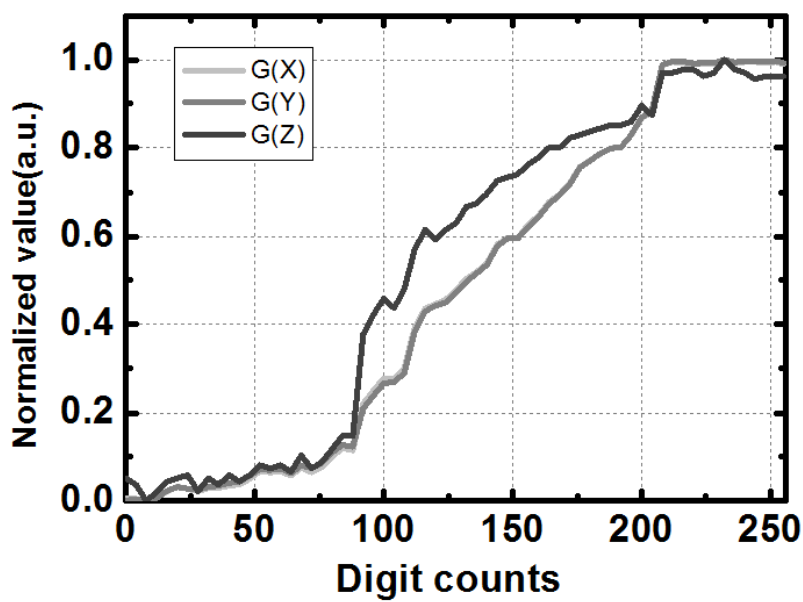
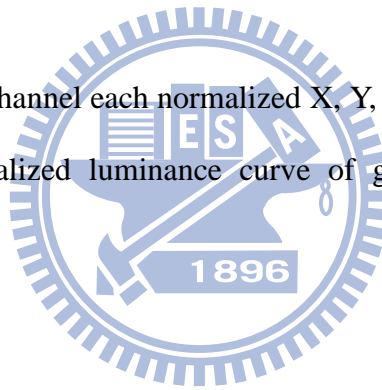


Fig. 4-5 Normalized X, Y, and Z values of green channel

32, 96, 192, and 255 gray level reflectance of each R, G, B channel were measured respectively to know whether three-layers stacked ChLCD has scalability or not. These three figures are shown below:

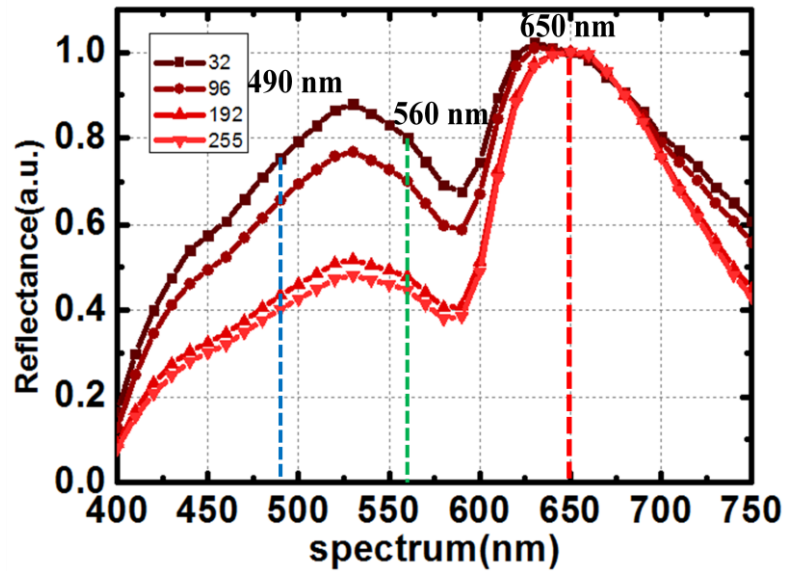


Fig. 4-6 Normalized reflectance of 4 digit counts in red channel

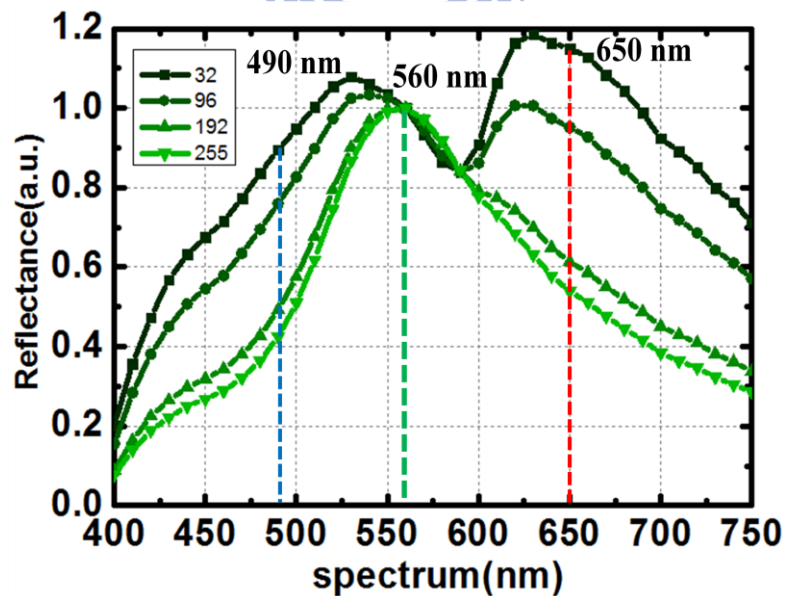


Fig. 4-7 Normalized reflectance of 4 digit counts in green channel

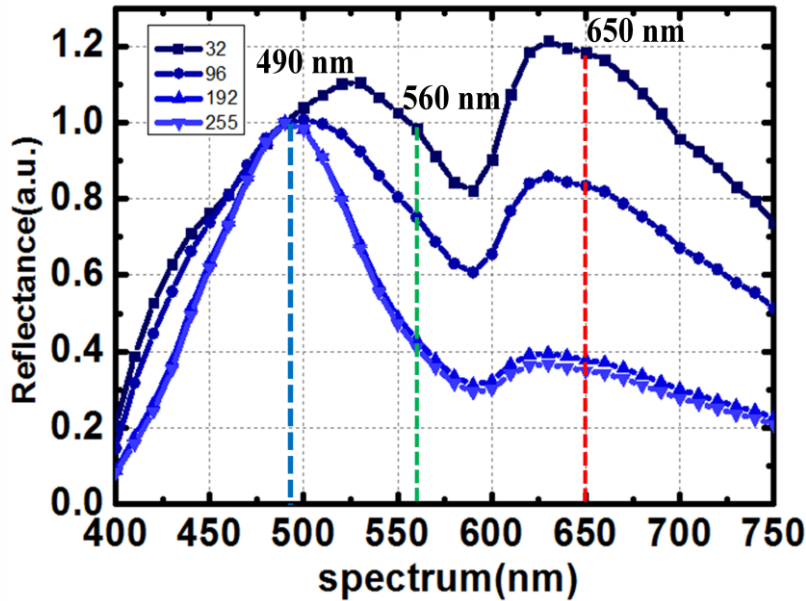


Fig. 4-8 Normalized reflectance of 4 digit counts in blue channel

These reflectance spectrum values of these three figures are normalized at dominant wavelength of each R, G, B channel which are 650, 560, and 490 nm, respectively. So, these normalized reflectance spectrum values are not scalable. Besides, the normalized reflectance spectrum figure of only green color taken for example is shown that high gray level fits well, but low gray level would be influenced by dominant wavelength of red and blue channel. So the spectra of green channel in low gray level also rise up in another wave band. Because few amount of the disordered liquid crystal in focal conic state may be regarded as planar state for a specifically oblique incidence or viewing angle. Red and blue layer introduce a little bit of reflection accordingly even the two layers are focal conic state. In addition, while some scattering contributed from the randomized cholesteric LCs is very weak, it did affect the color performance of ChLCDs. Because effective quantity of another two dominant wavelength is constant, these effective quantities may influence the reflectance spectrum in low gray level more remarkable than in high gray level. Another two channels are vice versa. Then, the figure of x, y values in CIE color

space with 32, 96, 192, and 255 digit counts of R, G, B channels and gray levels is illustrated as Fig. 4-9 (a), and the figure of x, y values in CIE color space with 32, 96, 192, and 255 digit counts of cyan (C), magenta (M), yellow (Y) is shown as Fig. 4-9 (b).

If the panel has scalability, no matter what the gray level of each R, G, B color channel is, x, y values should be the same or be little different. However, as Fig. 4-9 (a), they are not the same in this panel obviously. Moreover, x, y values in CIE color space with 32, 96, 192, and 255 digit counts of C, M, Y are also not at the same place respectively in Fig. 4-9 (b). So, physical model is not suitable for characterizing three-layers-stacked ChLCD. Another two methods will be given below.

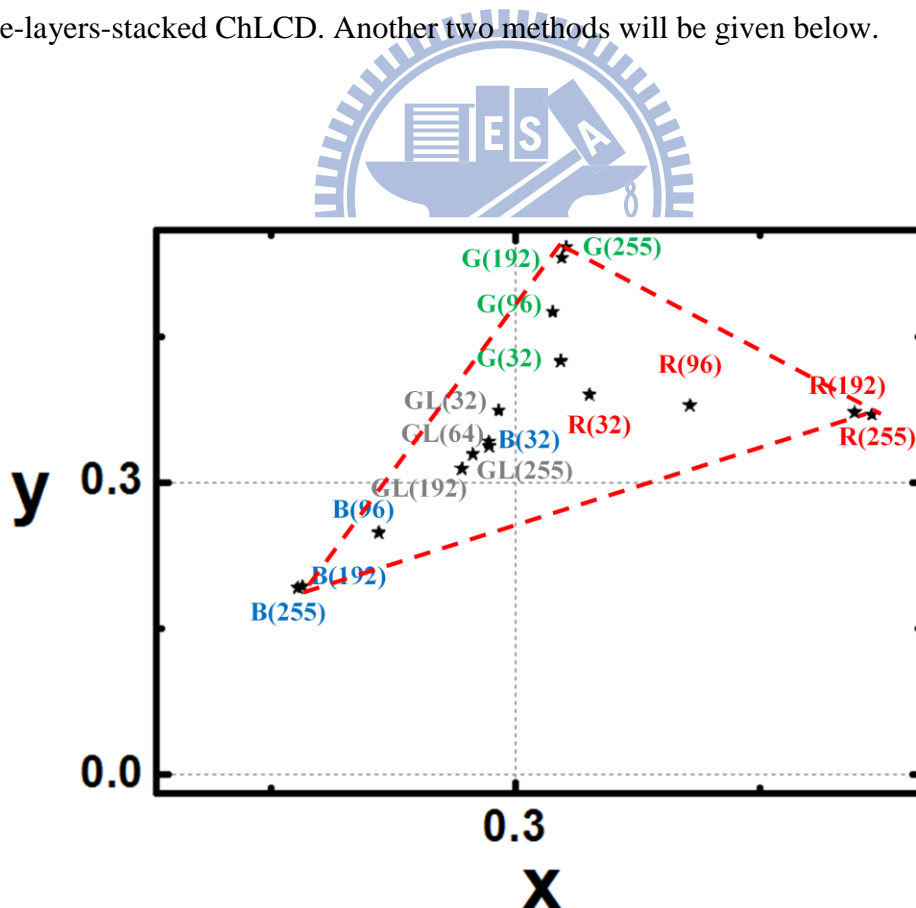


Fig. 4-9 (a) x,y values in CIE color space with 32, 96, 192, and 255 digit counts of R,G,B channels and gray levels

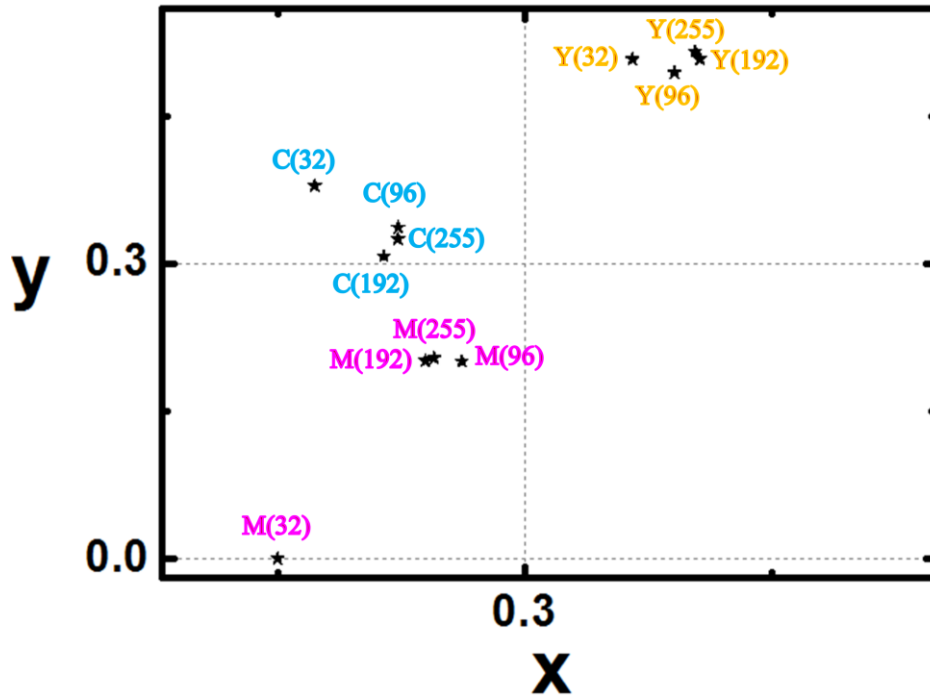


Fig. 4-9 (b) x,y values in CIE color space with 32, 96, 192, and 255 digit counts of cyan, magenta, yellow

4.3 Regression data with numerical model

The regression is from RGB digit counts to CIEXYZ. The flow chart of Fig. 3-8 is followed to decide how many terms of polynomial should be used. Finally, eight polynomials of Table 2-1 with three, four, six, eight, nine, eleven, fourteen, and twenty terms are utilized for the regression. The training sets which are the same with 9x9x9 LUT are a set of nine-level, unequally spaced lattice points (729 points) in the RGB space presenting in chapter 4.4. The testing sets are 900 randomized test samples in uniform color space of Fujitsu FLEPIa.

Fig. 4-10 (a) ~ (c) are shown the 900 randomized test color samples, the 900 randomized test samples in uniform a^*b^* color space of Fujitsu FLEPIa, and the distributions of lightness with the 900 randomized test samples. These figures can prove that 900 test samples are uniformly distributed in La^*b^* color space. Afterward,

eight polynomials of Table 2-1 with three, four, six, eight, nine, eleven, fourteen, and twenty terms are utilized for the regression. Table 4-3 lists the average CIEDE2000 color differences using these polynomials.

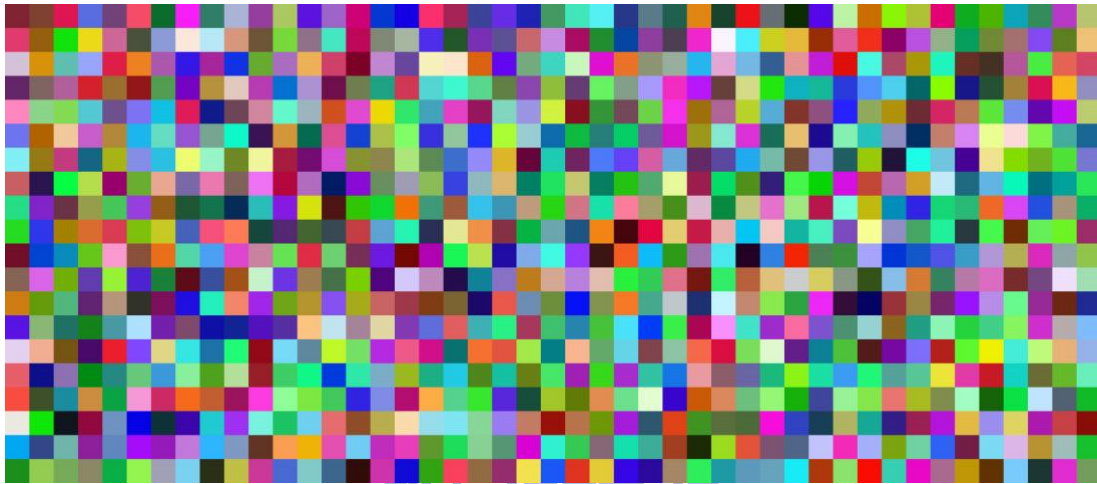


Fig. 4-10 (a) The 900 randomized test color samples

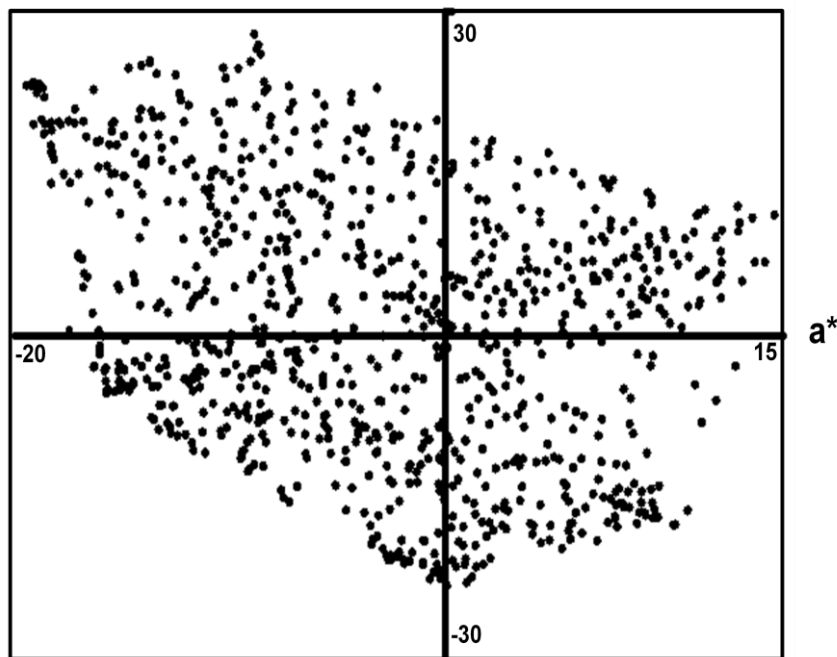


Fig. 4-10 (b) The 900 randomized test samples in uniform a^*b^* color space of

Fujitsu FLEPia

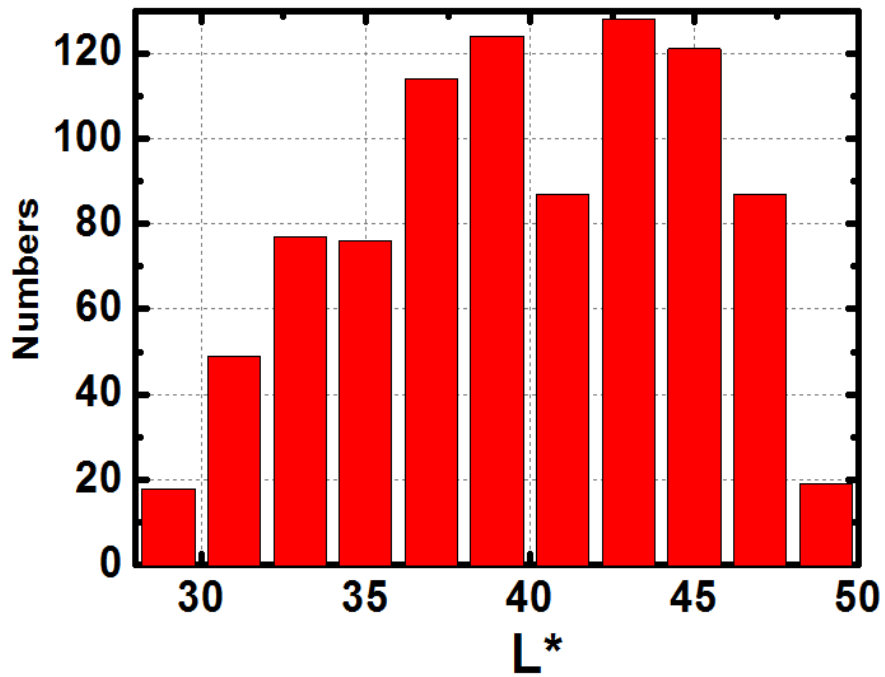


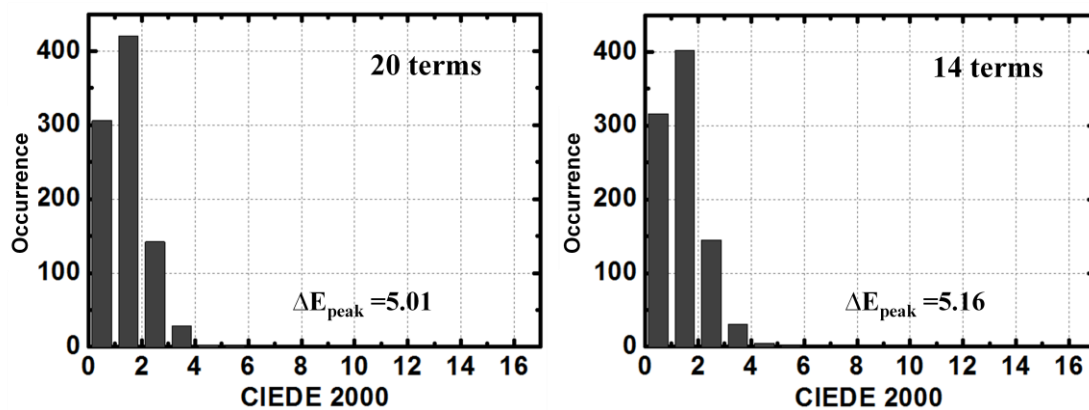
Fig. 4-10 (c) The distributions of lightness with the 900 randomized test samples

Table 4-3 Average CIEDE2000 color differences of various polynomial regressions

Polynomial term	Training	Testing	Total
3	4.68	3.67	4.12
4	3.47	2.63	3.01
6	3.87	2.91	3.34
8	3.73	2.92	3.28
9	3.17	2.49	2.79
11	2.76	2.19	2.45
14	1.51	1.41	1.45
20	1.5	1.4	1.44

Although the $\Delta E_{00_avg.}$ of training sets in polynomials of low terms is too high, the color differences of testing sets in these low terms polynomials still were calculated. These results of Table 4-3 show that the average CIEDE2000 color differences decreases as the number of terms in the polynomial increases except six and eight terms. The reason should be that usually the number of terms in the polynomial increases as the average color differences decreases, but it does has exception.

The distributions of CIEDE2000 color differences with testing sets are plotted in Fig. 4-11. The error distribution becomes narrow and shifts toward small CIEDE2000 color differences as the number of terms in the polynomial increases except 6, and 8 terms. Although the $\Delta E_{00_avg.}$ of 14, and 20 terms polynomials are below 1.5, the result is not good enough to predict the color performance of three-layers-stacked ChLCD. So, the LUT with interpolation method will be talked in the next section.



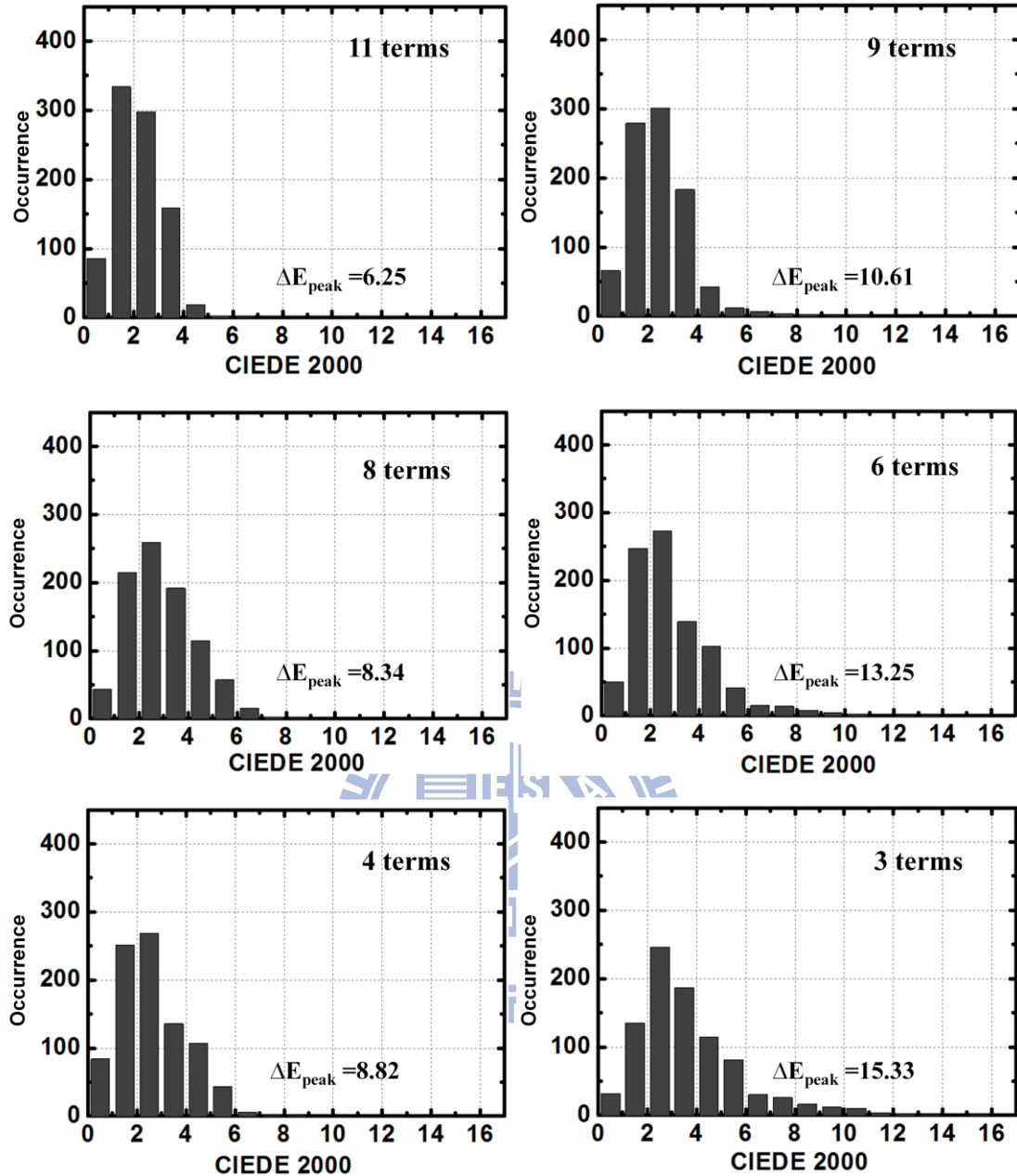


Fig. 4-11 Error distributions of regression

4.4 Interpolation from look-up tables

The first part of 3D LUT is packing. Depends on the gamma curve of FLEPia, cubic of 3, 5, 7, and 9 non-uniform packing is chosen by operating sequence of flow chart. Table 4-4 is shown the chosen packing points of RGB device space in cubic of 3, 5, 7, and 9 LUT, respectively. These points were selected is relying on the error which is lowest between the gamma curve of FLEPia and the curve of packing points

by piecewise linear method. Table 4-5 is illustrated these values of error.

Table 4-4 The chosen packing points in cubic of 3, 5, 7, and 9 LUT

Levels of LUT	Packing digit counts
3	0, 44, 255
5	0, 88, 116, 208, 255
7	0, 88, 96, 108, 116, 208, 255
9	0, 44, 88, 96, 108, 116, 196, 208, 255

Table 4-5 The error between the gamma curve of Fujitsu FLEPia with green channel and the curve of packing points

Levels of LUT	Error
3	0.689
5	0.267
7	0.258
9	0.097

The result of Table 4-5 can prove that the values of error decrease as levels of LUT increase. Fig. 4-12 is shown the gamma curve of G channel the predicting gamma curves of G channel with 3, 5, 7, 9 selected break points and piecewise linear interpolation. As levels of LUT increase, the fitting curve is like the gamma curve of FLEPia more. Then, these four different kinds of packing points would be substitute to four different kinds of geometric interpolation methods.

Finally, the CIEDE2000 color differences and $\Delta E_{00_avg.}$ of 900 randomized test

samples in uniform color space of Fujitsu FLEPIa between the measured values and the predicting values of different interpolation methods with various packing points would be calculated. Fig. 4-13~Fig. 4-16 are illustrated the error distributions of CIEDE2000 color differences of various four interpolation methods including different four packing. These figures can prove that the trends of error distributions with these four interpolation methods look like almost the same just having a little difference.

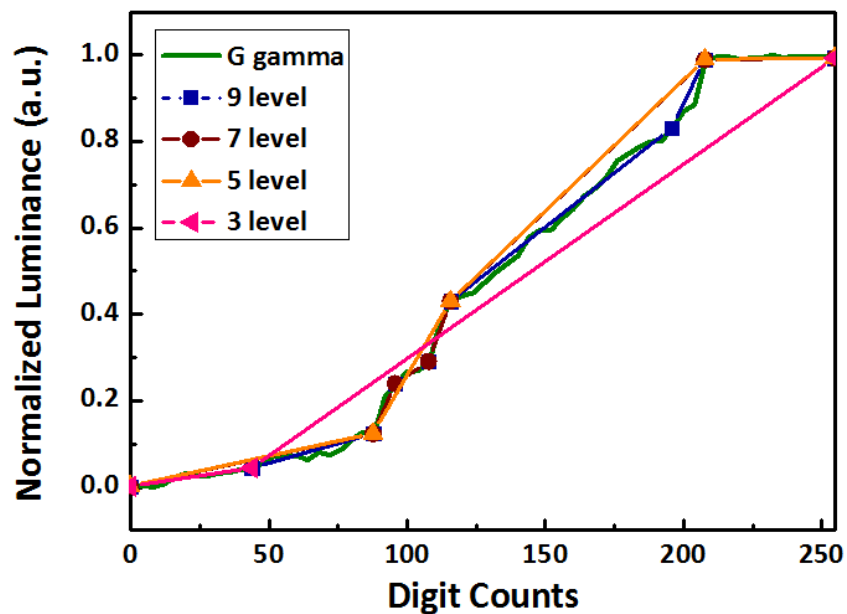
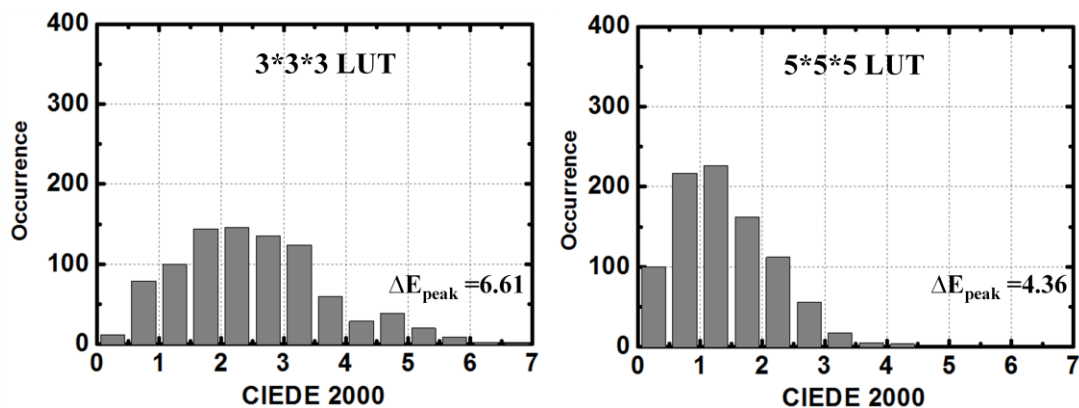


Fig. 4-12 The gamma curve of G channel and the predicting gamma curves of G channel with 3, 5, 7, 9 selected break points and piecewise linear interpolation



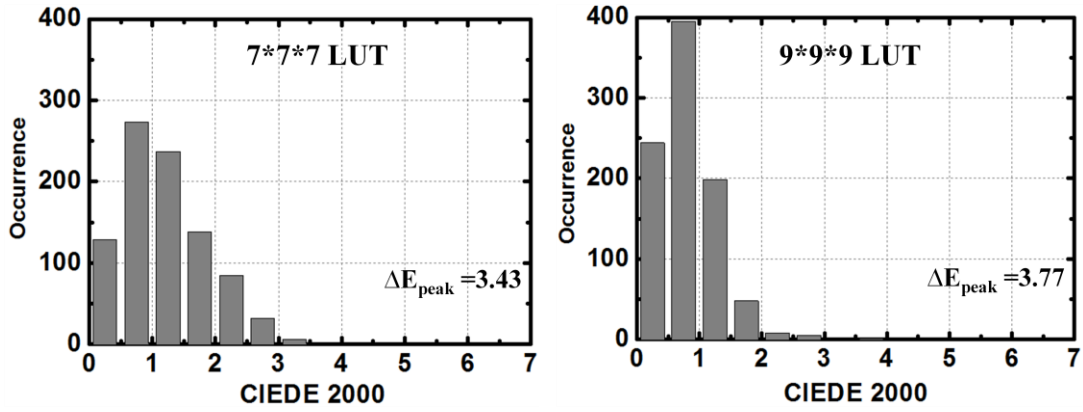


Fig. 4-13 The distribution of CIEDE2000 color differences
with trilinear interpolation

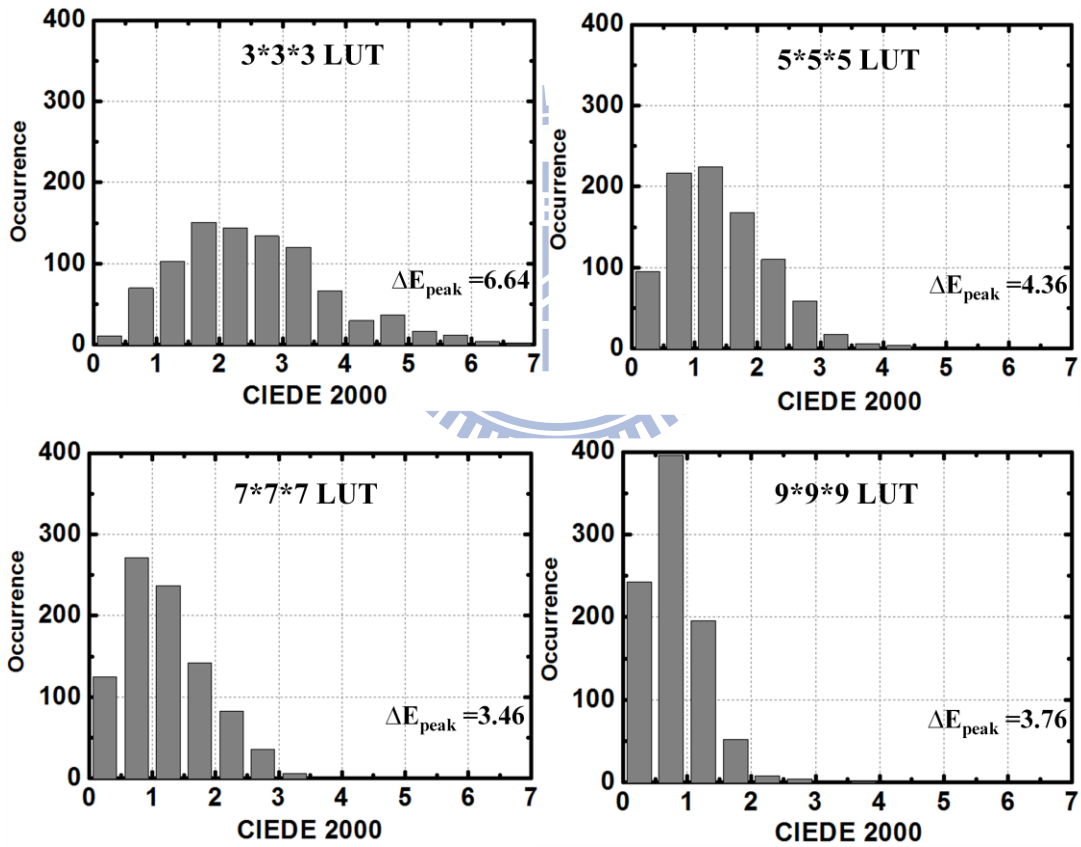


Fig. 4-14 The distribution of CIEDE2000 color differences
with prism interpolation

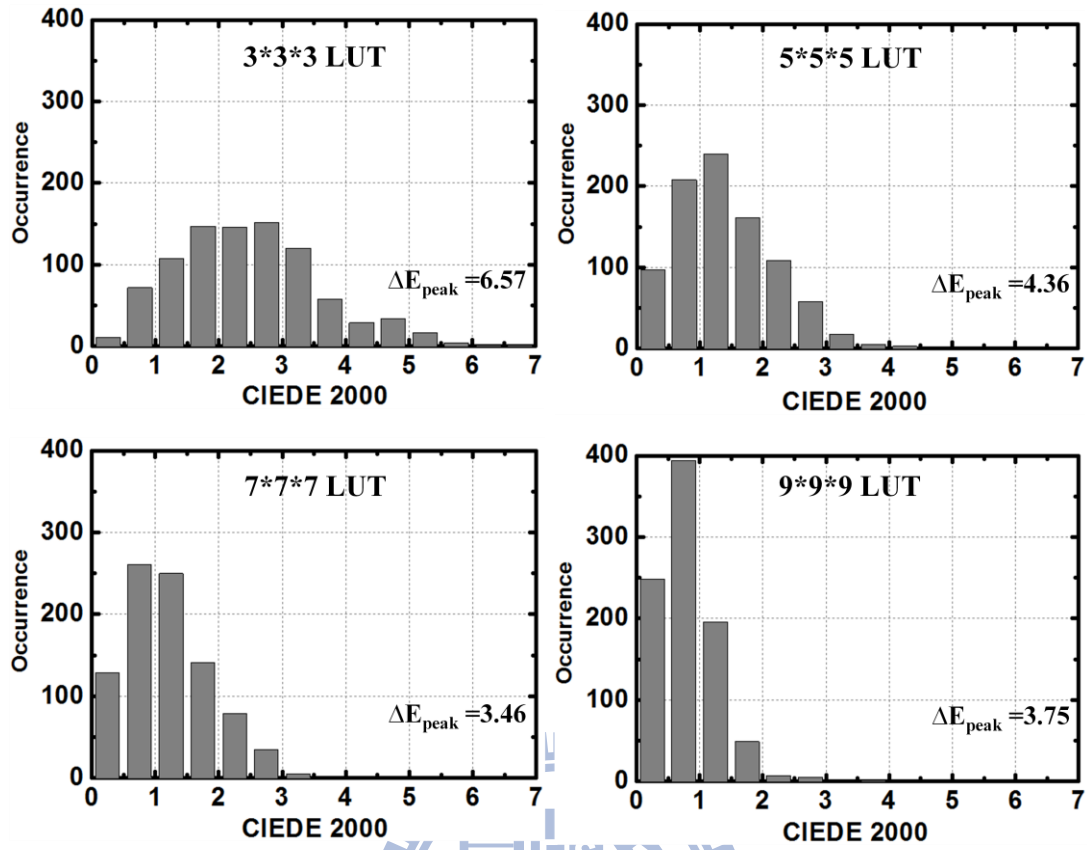
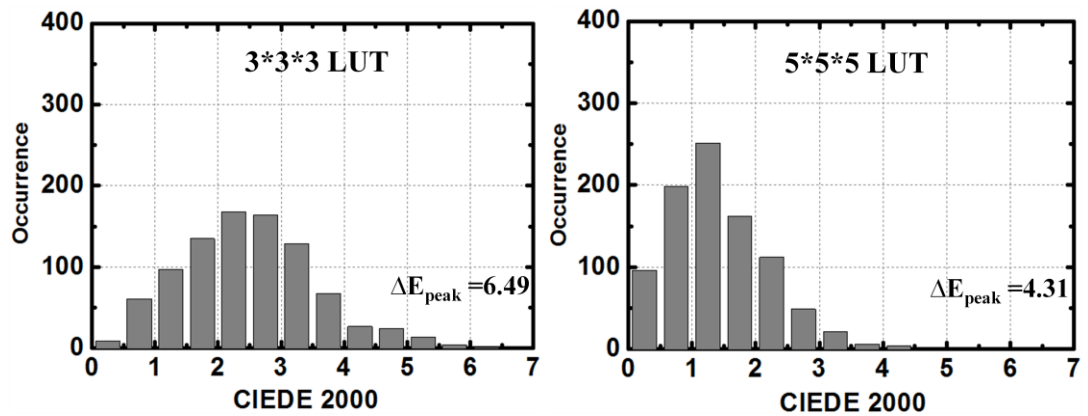


Fig. 4-15 The distribution of CIEDE2000 color differences with pyramid interpolation



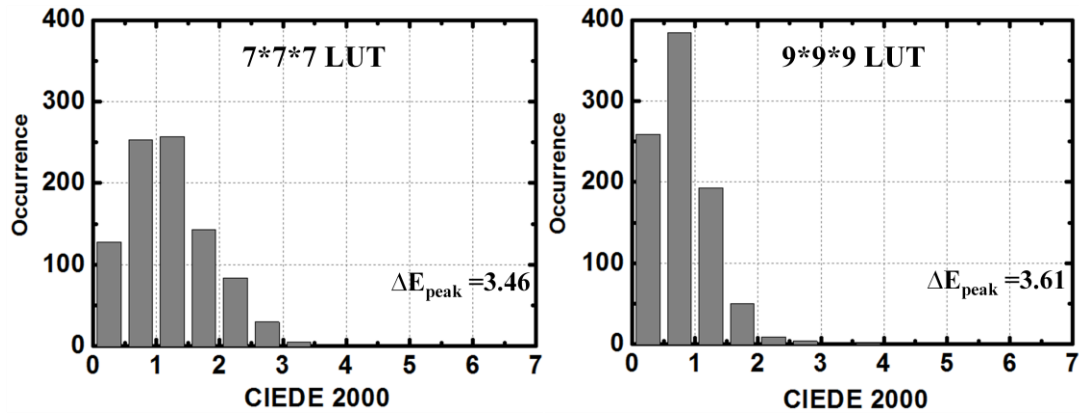


Fig. 4-16 The distribution of CIEDE2000 color differences with tetrahedral interpolation

These results from these figures showed that error amplitude decreases as the levels of LUT increase. The trend are illustrated that the error distribution becomes narrow and shifts to small CIEDE2000 color differences as the levels of LUT increase. Afterward, Table 4-6 is shown the average CIEDE2000 color differences between the measurement and predicting values of LUT.

Table 4-6 The average CIEDE2000 color differences between the measurement and predicting values of LUT

Packing numbers	Numbers of training sets	Trilinear	Prism	Pyramid	Tetrahedral
3	27	2.50	2.52	2.47	2.49
5	125	1.40	1.40	1.40	1.41
7	343	1.20	1.21	1.20	1.21
9	729	0.80	0.80	0.80	0.79

The results shown in Table 4-6 confirm that the interpolation accuracy improves as the sampling rate increases. At each packing, the interpolation accuracy

is about the same for different geometrical techniques. When the levels of packing numbers is from 7 to 9, the values of $\Delta E_{00_avg.}$ with various interpolation techniques are from near 1.2 to near 0.8 which is a great breakthrough. That means that the values of $\Delta E_{00_avg.}$ are below 1, humans cannot recognize. That is, LUT of non-uniform 9-level packing with various geometrical interpolation techniques successfully make the colorimetric characterization on three-layers-stacked ChLCD.

Finally, the comparison of storage and computation cost with four different 3D interpolations is illustrated as Table 4-7, where the computation cost of tetrahedral interpolation is most efficient in four different interpolation methods. From Table 4-6 and Table 4-7, LUT of non-uniform 9-level packing with tetrahedral interpolation would be the most efficient and accurate method to characterize ChLCD for this case.

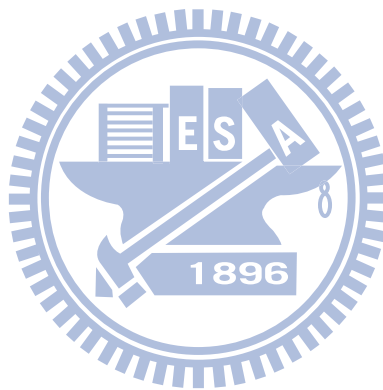
Table 4-7 Storage and computation cost of 3D interpolation for one component [12]

	Memory	Search	coefficient	Value
Trilinear	n^3	0	13(+/-)	10(\times/\div); 7(+/-)
Prism	n^3	1	7(+/-)	8(\times/\div); 5(+/-)
Pyramid	n^3	2	5(+/-)	7(\times/\div); 4(+/-)
Tetrahedral	n^3	2/3	3(+/-)	6(\times/\div); 3(+/-)

4.5 Summary

The physical model of colorimetric characterization on three-layers-stacked ChLCD is failed because its reflectance spectra have no scalability. Then, the numerical model with polynomials of three, four, six, eight, nine, eleven, fourteen, and twenty terms were used to characterize ChLCD. But the $\Delta E_{00_avg.}$ between the

predicted values by polynomials and the measured values of 900 testing sets are all behind one. So, numerical model with regression is not suitable for characterizing ChLCD. Finally, look-up tables are utilized to do the colorimetric characterization on ChLCD. The ΔE_{00_avg} of various four geometrical interpolation methods in cubic of 9 non-uniform packing are all below 1. This result proved that look-up tables with interpolation are the adequate method to characterize ChLCD. Furthermore, among these four interpolation methods, the most beneficial method is tetrahedral interpolation.



Chapter 5

Conclusions and Discussions

5.1 Conclusions

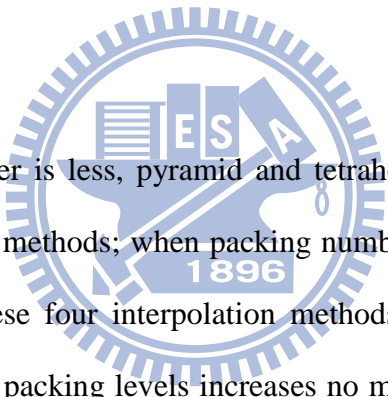
As the green issue has been thought of an important theme for discussion, the need for e-Paper will grow with each passing day. Full color e-Papers are the main stream of research now. When different types of e-Papers have come to maturity, the color mechanism of them maybe would become more and more complex.

The objective of this thesis is to construct the colorimetric characterization of e-Paper, and ChLCD is taken for our example. At first, the reflectance spectra of ChLCD were proved that they do not have scalability because of its complicated color performing system, so the physical model of colorimetric characterization is failed to present the color properties of ChLCD. And then, the numerical model on ChLCD would be shown next. Finally, the best method which is look-up table with interpolation to characterize ChLCD would be taken on.

Eight different polynomials with three, four, six, eight, nine, eleven, fourteen, and twenty terms are utilized for the regression, and the unequally spaced lattice points (729 points) in the RGB space are taken to be the training sets in the numerical model. Firstly, the color differences between the predicted values of regression polynomials of 729 training sets and the measured values would be calculated. Secondly, the color differences between the predicted by regression and the measured values of 900 randomized test samples in uniform color space would be calculated, too. Finally, we found that the error distribution becomes narrow and shifts toward

small CIEDE2000 color differences as the number of terms in the polynomial increases except 6, and 8 terms. Although the ΔE_{00_avg} of 20 terms is 1.44, its value is not good enough to present the color characteristic of ChLCD. So look-up table with interpolation also would be applied on colorimetric characterization of ChLCD.

At first, four various non-uniform packing methods are chosen, they are cubic of 3, 5, 7, and 9. And then, four different geometrical interpolation methods are used, they are trilinear, prism, pyramid, and tetrahedral. From calculating the ΔE_{00_avg} between the predicted values by these 16 various geometrical packing interpolation and measured values of 900 randomized test samples, the results can be summarized below.



When packing number is less, pyramid and tetrahedral interpolation methods are better than another two methods; when packing number is more, there are nearly no differences between these four interpolation methods. And the error amplitude decreases as the number of packing levels increases no matter which the geometrical interpolation method is. Finally, the ΔE_{00_avg} of these four geometrical interpolation methods in cubic of 9 non-uniform packing are below 1, which means humans cannot recognize these differences. Namely, LUT of non-uniform 9-level packing with various geometrical interpolation techniques successfully make the colorimetric characterization on three-layers-stacked ChLCD. Among these four different interpolation methods, the most beneficial and accurate method is tetrahedral interpolation for our case.

In the near future, no matter what the complex e-Paper or even any display is, these series of colorimetric characterization methods could be completely imitated on

it. Then, the best way can be found to be utilized on it.

5.2 Discussions

Although ChLCD has been developed with full color technology, its color performance has a deadly disadvantage which is color shift owing to viewing angle shift. Because its reflective light wavelength obeys Bragg's law ($\lambda = n \cdot p \cdot \cos\phi$, λ : wavelength of reflective light, n : refractive index, p : pitch of ChLC, ϕ : incident angle), as ϕ increases, corresponding λ decreases; as ϕ decreases, corresponding λ increases. Fig. 5-1 is a diagram taking for an example to show this phenomenon. When viewing geometry changes from $45^\circ/0^\circ$ to $45^\circ/+10^\circ$ and $45^\circ/-10^\circ$, it can be taken as $55^\circ/0^\circ$ and $35^\circ/0^\circ$. The observed light wavelength would change from long wavelength to short wavelength (blue shift) when viewing geometry changes from $45^\circ/0^\circ$ to $45^\circ/+10^\circ$; from short wavelength to long wavelength (red shift) when viewing geometry changes from $45^\circ/0^\circ$ to $45^\circ/-10^\circ$. This phenomenon is still opened for future study.

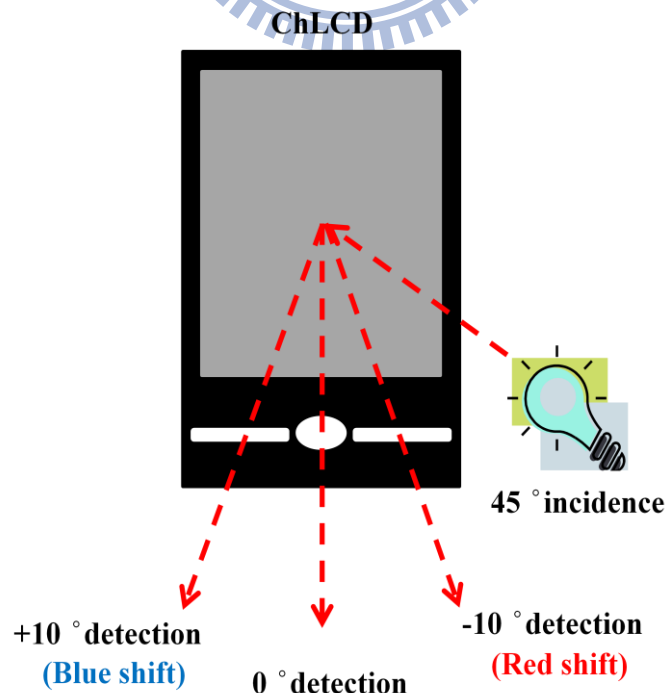


Fig. 5-1 A diagram of ChLCD color shift

Reference

1. G. H. Gelinck, *et al.*, “A rollable, organic electrophoretic QVGA display with field-shielded pixel architecture,” *JSID* 14/2, 113–118 (2006).
2. A. M. Green, *et al.*, “Energy efficient flexible Reflex™ displays,” *Proc. IDRC '08*, 55–59 (2008).
3. J. Heikenfeld, *et al.*, “Review Paper: A critical review of the present and future prospects for electronic paper,” *JSID* 19/2, 131 (2011).
4. P. Green, *et al.*, “Colour Engineering- Achieving Device Independent Colour,” *John Wiley & Sons, Ltd.*, 127-129 (2002).
5. J. Morovic, “Color Gamut Mapping,” *John Wiley & Sons, Ltd.*, 45-47 (2008).
6. 胡國瑞等, “顯示色彩工程學,” *全華圖書股份有限公司*, 139 (2009).
7. E. F. Schubert, “Light Emitting Diode,” Second Edition, *Cambridge University Press*, 313-348 (2006)
8. A. A. Afifi, *et al.*, “Statistical Analysis,” *New York: Academic Press*, 108 (1972)
9. H. R. Kang, “Color scanner calibration of reflected samples,” *Proc. SPIE 1670*, 468-477 (1992)
10. H. R. Kang, *et al.*, “Neural network applications to the color scanner and printer calibrations,” *J. Electron. Imag.*, Vol. 1: 125-135 (1992)
11. J. M. Kasson, *et al.*, “A tetrahedral interpolation technique for color space conversion,” *Proc. SPIE 1909*, 127-138 (1993)
12. H. R. Kang, “Color Technology for Electronic Imaging Devices,” *SPIE Optical Engineering Press*, 67-150 (1997)
13. P. C. Hung, “Colorimetric calibration in electronic imaging devices using a look-up-table model and interpolations,” *Journal of Electronic imaging* 2(1),

- 53-61 (1993)
14. H. C. Lee, "Introduction to Color Imaging Science," *Cambridge University Press*, 401 (2005)
 15. X. Y. Huang, *et al.*, "The transient response and dynamic drive of cholesteric liquid-crystal displays," *JSID5/3* , 179 (1997)
 16. S. T. Wu, *et al.*, "Reflective Liquid Crystal Displays," *John Wiley & Sons, Ltd.*, 208 (2001)
 17. D. Davis, *et al.*, "Eight-color high-resolution reflective cholesteric LCDs," *SID Intl. Symp. Digest Tech. Papers*, 29, 901 (1998)
 18. D. K. Yang, *et al.*, "Control of the reflectivity and bistability in displays using CLC," *J. Appl. Phys.* 76 (2), 1331 (1994)
 19. D. Davis, *et al.*, "Multiple color high resolution reflective cholesteric liquid crystal displays," *SID* (1997)
 20. A. Khan, *et al.*, "Recent progress in flexible color reflective cholesteric displays," *JSID16/2* , 245 (2008)
 21. J. P. Allebach, *et al.*, "Efficient implementation of nonlinear color transformations," *First IS&T/SID Color Imaging Conference: Transforms & Transportability of Color*, 143-148 (1993)
 22. <http://en.wikipedia.org/wiki/FLEPIa>
 23. http://www.xrite.com/product_overview.aspx?ID=1161